Observer-based Adaptive Finite-Time Neural Control for Constrained Nonlinear Systems With Actuator Saturation Compensation

Kang Liu, *Member, IEEE*, Po Yang, *Senior Member, IEEE*, Lin Jiao, *Member, IEEE*, Rujing Wang, Zhipeng Yuan, *Student Member, IEEE*, and Tao Li, *Member, IEEE*

***Abstract*—This brief designs an observer-based adaptive finite-time neural control for a class of constrained nonlinear systems with external disturbances, and actuator saturation. First, a neural network (NN) state observer is developed to estimate the unmeasurable states. Combining the improved Gaussian function and an auxiliary compensation system, the actuator saturation can be solved. The "*explosion of complexity*" problem is tackled by the finite-time command filter, and the filtering-error compensation system is constructed to resolve the filtering error. Moreover, the barrier Lyapunov function is incorporated into the controller design to satisfy the state constraints. By integrating the NN technique and the virtual parameter learning to approximate the bound of the lumped disturbance, the number of learning parameters is decreased. It can be proved that all the states do not transgress the predefined bounds and the tracking errors converge to bounded regions in finite time. Eventually, we provide comparative results to show the feasibility of the obtained results.**

***Index Terms*—Actuator saturation, full-state constraints, finite-time control, neural networks, state observer.**

ABBREVIATIONS

BC	Backstepping control
DSC	Dynamic surface control
CFB	Command filtered backstepping
NN	Neural network
RBFNN	Radial basis function NN
FTC	Finite time control
ACS	Auxiliary compensation system
BLF	Barrier Lyapunov function
FTCF	Finite-time command filter
ACFBC	Adaptive command filtering BC

Kang Liu, Po Yang, and Zhipeng Yuan are with the Department of Computer Science, University of Sheffield, Sheffield S10 2TN, U.K., (e-mail: k_liu@ieee.org;po.yang@sheffield.ac.uk; zhipeng.yuan@sheffield.ac.uk).

Lin Jiao is with the School of InterNet, Anhui University, Hefei 230031, China, (e-mail: ljiao@ahu.edu.cn)

Rujing Wang is with the Institute of Intelligent Machines, Hefei Institutes of Physical Science, Chinese Academy of Sciences, Hefei 230031, China, and also with University of Science and Technology of China, Hefei 230026, China, (e-mail: rjwang@iim.ac.cn).

Tao Li is with the College of Railway Transportation, Hunan University of Technology, Zhuzhou 412007, China, and also with the College of Mechanical and Vehicle Engineering, Hunan University, Changsha 410082, China, (e-mail: litao@hut.edu.cn).

I. INTRODUCTION

BACKSTEPPING technology as a recursive Lyapunov policy has attracted wide attention, and many constructive results have been reported to control nonlinear systems in [1]–[5]. However, the "*explosion of complexity*" issue severely hinders the application of backstepping control (BC) [1]. To overcome this issue, a dynamic surface control (DSC) was primarily in [2] by using the low-pass filter to approximate the derivative of the virtual control law in each iteration. In [3], the event-triggered DSC was investigated for autonomous surface vehicles. However, the DSC does not consider the filtering errors, which could destroy the system performance.

To circumvent the filtering error, the command filtered backstepping (CFB) was developed via the error compensation mechanism (see [6]–[9]). The work [6] initially discussed the impact of the command filter for the system stability, and then, this team presented an adaptive BC for the land vehicles [7]. Hao *et al.* [8] developed a multi-objective CFB for the active suspension systems. However, the above approaches are not adequate for nonlinear systems with unknown functions. By means of high reliability and strong approximation, a composite neural control was proposed to reduce the system errors and avoid high-frequency oscillations [10]. By applying the nonlinear transformed function, a command-filtered neural controller was presented in [11]. In [12], fuzzy technology was applied to the framework of the adaptive radial basis function NN (RBFNN). Although the above controllers-based NN technology can achieve good performance, it is not a straightforward way to update the NN's weight, which is because the controller requires many learning parameters. In particular, the number of learning parameters obviously grows as the weight dimension of the NN grows. This leads to high computational load and approximation errors. As an alternative method, a neuron-adaptive learning policy was presented in [13], but many threshold parameters are difficult to choose. In this setting, it is meaningful for the design of NN control with a lower computational burden.

The aforementioned works only consider the system states that can be directly measured and observed, which prevents the state-feedback controller from being implemented smoothly [14]. To solve the obstacle induced by unmeasurable states, a linear state observer was integrated into the adaptive NN controller [15]. But, most systems are nonlinear, and the linear observer has limitations in theory and practice. A piecewise

observer was constructed to observe the system states [16]. The CFB combined with the neural state observer was considered [17]. Even though many conclusions have been developed to estimate the unavailable states, the convergence time cannot be reached as the time goes to finite. For this point, the control goal requires that the errors are close to the equilibrium when the time approaches infinity, such as the rigid spacecraft [18], quadrotor systems [19], and manipulators [20], etc. In [21], *Bhat* and *Bernstein* developed pioneering results in the finite-time control (FTC), which is a generalization for nonlinear systems that do not conform to the Lipschitz condition. After that, the study [22] discussed the FTC matters for linear systems, while the study [23] considered the FTC matters for nonlinear systems. The traditional FTCs require that the Lyapunov function $V(\cdot)$ satisfies $\dot{V}(\cdot) \leq aV^b(\cdot) + \varrho_1$ with $a < 0$, $0 < b < 1$ and $\varrho_1 \geq 0$ [21], [22], [24], however its convergence rate is even lower than that of $\dot{V}(\cdot) \leq cV(\cdot) + \varrho_2$ with $c < 0$ and $\varrho_2 \geq 0$ when the function $V(\cdot)$ becomes large [25]. To accelerate the convergence rate, a criterion called fast finite-time stability is proposed and satisfies $\dot{V}(\cdot) \leq cV(\cdot) + aV^b(\cdot) + \varrho$ with $\varrho \geq 0$ [9], [27]–[29], which has been extensively applied, such as the study [20] designed the DSC method for the manipulator system, and the study [30] proposed an observer-based neural control to realize a faster arrival time. From the above analysis, the study on the fast FTC problem is very important for the controller design, hence this is what we are committed to focusing on.

In practice, various constraints such as actuator saturation and state constraints are common [31]–[34]. Once these constraints can not be tackled properly, it would cause system instability. The smooth function was introduced to approximate the saturation function at the sharp corners [5], but the approximation error is ignored. To solve this problem, Yu *et al.* [26] adopted the Nussbaum-type function to compensate for the nonlinear term. As an alternative manner, an auxiliary compensation system (ACS) was constructed to mitigate the effects of the input saturation [35], [36], but it can not handle the issue that the control input is not smooth. In [37], the designed ACSs can address the input saturation effectively, but they require that the input deviation is supposed to be bounded. In [32], the smooth function was adopted to obtain a smooth control law, and the difference between the control law and the output of the smooth function was utilized to drive the ACS. Although the above approaches can resolve the input saturation, there is still room for improvement. For the system constraint problem, Tee *et al.* [38] applied the barrier Lyapunov function (BLF) to guarantee that the output constraint is never violated. Zhao *et al.* [39] studied an adaptive NN controller for uncertain helicopters with output constraints. Compared to just considering the output constraint. To do this, Zhang *et al.* [24] proposed a fuzzy FTC to avoid the violation of full-state constraints. Liu *et al.* [40] designed a BLF-based FTC to address the full-state constraints and nonaffine terms. An adaptive fuzzy controller was presented in [41] for the permanent magnet synchronous motors. In [42], the integral BLF-based backstepping control was investigated, but the problem of feasibility condition is still not solved.

By synthesizing the above observations, we will design an observer-based adaptive finite-time neural controller for constrained nonlinear systems subject to unmeasurable states, external disturbances, and actuator saturation. The primary innovations of this study are highlighted, as

(1) Unlike the multi-objective adaptive CFB [8], the neural CFB [10], and the event-triggered DSC [3], the proposed controller, which integrates the CFB technology and the filtering-error compensation system, not only solves the problems of "*explosion of complexity*" and the filtering error but also realizes the fast finite time convergence. Compared to previous studies in [1]–[3], [20], [36], this study does not require the availability of system states, which means that the state observation and the controller can be designed independently. This makes proposed controller more flexible for practical applications.

(2) To approximate the actuator nonlinearity, this study designs an improved Gaussian function that provides a higher approximation accuracy than the continuous functions in [26], [32]. Different from previous studies in [32], [35]–[37] to solve the saturation-approximation error, the designed ACS not only quickly eliminates the saturation effect Δu without the boundedness of Δu but also guarantees the smooth output of the ACS and avoids the singularity problem. Moreover, the BLFs are integrated into each step of the controller design so that all states are kept within the predefined sets.

(3) By combining the NN technique and the virtual learning parameter to compensate for external disturbances and nonlinear functions, the computational burden is reduced due to fewer learning parameters in comparison with the traditional NN controllers [30], [35], [39]. Thus, this helps to extend the controller to other controlled systems.

The remaining sections are arranged as: The problem formulation is described in Section II. Section III gives the steps of the controller development and the convergence analysis. Section IV illustrates the validity of the proposed scheme, and then Section V to give the conclusions.

II. Problem Preliminaries

A. System Description

Consider a class of constrained nonlinear systems, as

$$\begin{cases} \dot{x}_i = & f_i(x) + g_i x_{i+1} + d_i(t) \\ \dot{x}_n = & f_n(x) + g_n \tau + d_n(t) \\ y = & x_1, \quad i = 1, \cdots, n-1 \end{cases} \tag{1}$$

where $\bar{x}_i = [x_1, \ldots, x_i]^{\mathrm{T}}$ and $x = [x_1, \ldots, x_n]^{\mathrm{T}}$ are system states; $\bar{x}_1 = x_1$, $\bar{x}_n = x$; $f_i(x)$ and $f_n(x)$ are the unknown functions; g_i and g_i are known nonzero functions; $d_i(t)$ and $d_n(t)$ are the external disturbances and satisfy $d_i(t), d_n(t) \leq \bar{d}$ with $\bar{d} > 0$ being an unknown scalar; $f_i(x)$ and $f_n(x)$ are system uncertainties; τ and y are the control input subject to the saturation and control output, respectively; Let $F_i(\bar{x}_i) = f_i(x) + d_i(t)$ and $F_n(x_n) = f_n(x) + d_n(t)$ be lumped disturbances. All states are constrained in a compact set, that is, there is a constant $k_{ai} > 0$ such that $|x_i| \leq k_{ai}$.

Remark 1: Apart from the theoretical concerns, the system (1) is more general than the systems considered in [30], [40]

due to the simultaneous consideration of external disturbances, actuator saturation, and full-state constraints. Moreover, many physical systems can be transformed into (1) by proper state transformations, such as mechanical manipulators [20], land vehicles [7], helicopters [39], spacecraft systems [18], etc.

Since the actuator saturation is a widespread problem in actual systems, the control input τ is considered as

$$\tau = \text{sat}(u) = \begin{cases} \bar{u}_r, & \text{if } u > \bar{u}_r \\ u, & \text{if } \underline{u}_l \le u \le \bar{u}_r \\ \underline{u}_l, & \text{if } u < \underline{u}_l \end{cases} \tag{2}$$

where u is the actual control input; $\bar{u}_r > 0$ and $\underline{u}_l < 0$ are the upper and lower bounds of u. However, since τ is a piecewise function with nonsmooth nonlinearity, the backstepping technique cannot be applied directly. For resolving this issue, this study introduces an improved Gaussian function to approximate the saturation nonlinearity via the work [32], as

$$h(u) = u^* \mathcal{H}\left(\frac{\sqrt{\pi}u}{2u^*}\right) \tag{3}$$

where the function $\mathcal{H}(\bullet)$ is denoted as $\mathcal{H}(\bullet) = \frac{2\varphi_1}{\sqrt{\pi}} \int_0^{\bullet} \exp^{-\varphi_2 x^2} dx$ with $\varphi_1 > 0$ and $\varphi_2 > 0$ being adjustable parameters, and $u^* = 0.5(\bar{u}_r + \underline{u}_l) + 0.5(\bar{u}_r - \underline{u}_l)\,\text{sign}(u)$.

Due to the existence of approximation error, $h(u)$ cannot completely substitute $\text{sat}(u)$ in (2). Further, it is reasonable that $\text{sat}(u)$ can be rewritten by $\text{sat}(u) = h(u) + \Delta u$, where the approximation error Δu can be constrained by

$$|\Delta u| = |\text{sat}(u) - h(u)| \le \Delta \bar{u} \tag{4}$$

in which $\Delta \bar{u} > 0$ represents an unknown constant. From the mean-value theorem, the function $h(u)$ can be rewritten by

$$h(u) = h(\breve{u}) + \kappa(u - \breve{u}) \tag{5}$$

where $\kappa = \frac{\partial h(u)}{u}|_{u=u^{b_0}} = \exp\big(-(\sqrt{\pi}u^{b_0})/(2u^*)\big) \in (0, 1]$, $u^{b_0} = b_0 u + (1 - b_0)\breve{u}$ and $0 < b_0 < 1$. By considering $h(0) = 0$ for $\breve{u} = 0$, one has

$$\text{sat}(u) = \kappa u + \Delta u \tag{6}$$

where $\kappa > 0$ represents a computable variable.

Remark 2: The models of symmetric saturation and asymmetric saturation can be built by changing the values of $\bar{u}_r$ and $\underline{u}_l$. If $|\bar{u}_r| = |\underline{u}_l|$, it is symmetric saturation model; else if $|\bar{u}_r| \neq |\underline{u}_l|$, it is symmetric saturation model. Although the function $\mathcal{H}(\bullet) = \frac{2}{\sqrt{\pi}} \int_0^{\bullet} \exp^{-x^2} dx$ in [32] provides higher approximate accuracy than the hyperbolic tangent function [26], its approximation error can not be adjusted to small enough. To solve this challenge, an improved Gaussian function (3) is introduced. As an example, it can be observed that from the enlarged part of Fig. 1, the function (3) indeed solves the actuator saturation with symmetric and asymmetric cases,

Assumption 1: (*See [25]*) The desired trajectory y_d and its derivative $\dot{y}_d$ are known and bounded signals, that is, y_d and $\dot{y}_d$ satisfy $|y_d| \le Y_1$ and $|\dot{y}_d| \le Y_2$ with Y_1 and Y_2 being positive and known constants.

Assumption 2: (*See [25]*) The function $g_i(\bar{x}_i)$ for $1 \le i \le n$ is unknown but its sign is known, and there exists two constants $\underline{g} > 0$ and $\bar{g} > 0$ hold the following:

$$0 < \underline{g} \le |g_i(\cdot)| \le \bar{g}. \tag{7}$$

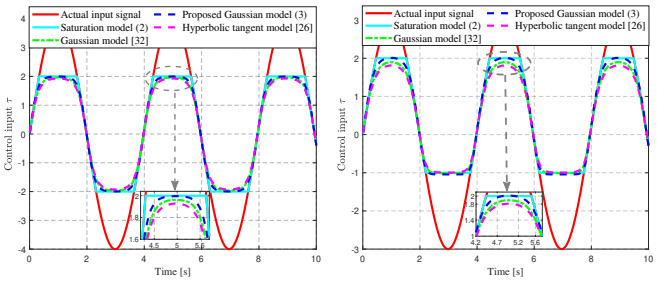

(a) Symmetric saturation model (b) Asymmetric saturation model

Fig. 1. Curves of control input τ and its saturation: (a) $\bar{u}_r = 2$, $\underline{u}_l = -2$ and $u(t) = 4\sin(1.6t)$; (b) $\bar{u}_r = 2$, $\underline{u}_l = -1$, and $u(t) = 3\sin(1.6t)$.

where $g_i(\cdot)$ is strictly positive or negative. Without loss of generality, $g_i(\cdot)$ is supposed to be strictly positive.

Remark 3: Some explanations are stated about Assumptions 1 and 2: (i) Compared with approximation-based BC schemes [26], [29], where the knowledge of $y_d^j(t)$, $j = 0, 1, \ldots, n$ is needed, Assumption 1 only requires $y_d(t)$ and its derivative to be bounded, which means that the controller is less constrained and is more suitable for high-order systems. (ii) Assumption 2 is general such as [11], [25], and $\underline{g}$ and $\bar{g}$ are only used to analyze the system stability rather than the controller design. Therefore, the given assumptions are reasonable.

Lemma 1: (*See [39]*) For any positive constant $k_b \in \mathbb{R}$ and any vector $z \in \mathbb{R}^n$ with $\|z\| \le k_b$, one obtains

$$\log \frac{k_b^2}{k_b^2 - z^{\mathrm{T}} z} \le \frac{z^{\mathrm{T}} z}{k_b^2 - z^{\mathrm{T}} z}. \tag{8}$$

Lemma 2: (*See [40]*) Consider the nonlinear system, as

$$\dot{x} = f(x, u), \quad f(0, 0) = 0, \quad x \in \mathbb{R}^n, \quad u \in \mathbb{R}^m \tag{9}$$

wherein x and u are the state and input vectors, respectively, and $f : W \to \mathbb{R}^n$ is continuous on an open neighbourhood W. If there is a Lyapunov function $V(x)$ as $\dot{V}(x) \le -\pi_1 V(x) - \pi_2 V^{\pi_3}(x) + \pi_4$, $\forall t > t_0$ with $0 < \pi_4 < \infty$, $\pi_1 > 0$, $\pi_2 > 0$ and $0 < \pi_3 < 1$, the system (9) is fast finite-time stability and drives into the bounded region, as

$$\Omega = \left\{ \lim_{t \to T} V(x) \le \min\left\{ \frac{\pi_4}{(1 - \iota)\pi_1}, \left(\frac{\pi_4}{(1 - \iota)\pi_2}\right)^{\frac{1}{\pi_3}} \right\} \right\} \tag{10}$$

where $0 < \iota < 1$, and the convergence time is estimated as

$$T \le t_0 + \max\left\{ \frac{1}{\iota\pi_1(1 - \pi_3)} \ln \frac{\iota\pi_1 V^{1-\pi_3}(t_0) + \pi_2}{\pi_2}, \frac{1}{\pi_1(1 - \pi_3)} \ln \frac{\pi_1 V^{1-\pi_3}(t_0) + \iota\pi_2}{\iota\pi_2} \right\} \tag{11}$$

where t_0 is the initial time.

Lemma 3: (*See [30]*) There are two constants $p > 0$ and $q > 0$, and a real-valued function $o(x, y)$ such that

$$|x|^p |y|^q \le \frac{po(x, y)|x|^{p+q}}{p + q} + \frac{qo(x, y)^{-\frac{p}{q}}|y|^{p+q}}{p + q}. \tag{12}$$

Lemma 4: (*See [24]*) Consider a given constant $0 < m \le 1$ and any vector $w = [w_1, \ldots, w_n] \in \mathbb{R}^n$, it follows that

$$\left(\sum_{i=1}^{n} |w_i|\right)^m \le \sum_{i=1}^{n} |w_i|^m \le n^{1-m} \left(\sum_{i=1}^{n} |w_i|\right)^m. \tag{13}$$

Lemma 5: (*See [43]*) The finite-time command filter (FTCF) is applied via the following form:

$$\begin{aligned}\dot{\vartheta}_1 =& -L_1|\vartheta_1-\alpha|^{\frac{1}{2}}\mathrm{sign}(\vartheta_1-\alpha)+\vartheta_2\\ \dot{\vartheta}_2 =& -L_2\mathrm{sign}(\vartheta_2-\dot{\vartheta}_1)\end{aligned} \tag{14}$$

where α and ϑ_1 are the virtual signal and the output signal of the filter, $L_1>0$ and $L_2>0$ are the filter's gains, and $\vartheta_1(0)\geq 0$ and $\vartheta_2(0)\geq 0$. There are two cases: If α is not disturbed by noises, it satisfies $\vartheta_1=\alpha_0$ and $\dot{\vartheta}_1=\dot{\alpha}_0$ after finite time, where $\alpha=\alpha_0$; else if α is not disturbed by noises, it satisfies $\vartheta_1=\alpha_0$ and $\dot{\vartheta}_1=\dot{\alpha}_0$ after finite time.

B. RBFNN Approximation System

As we know, the RBFNN technique is extensively applied to control the nonlinear system $f(Z)$, i.e.,

$$f(Z)=W^{*\mathrm{T}}\Xi(Z)+\zeta(Z),\quad \|\zeta(Z)\|\leq\bar{\zeta} \tag{15}$$

where W^*, $\delta(X)$, and $\bar{\zeta}$ are the ideal weight vector, approximation error, and positive scalar, respectively. From theoretical perspective, the ideal weight vector W^* can be given by

$$W^*=\arg\min_{W\in\mathbb{R}^{s\times m}}\left\{\sup_{Z\in\Omega}\left|f(Z)-W^{\mathrm{T}}\Xi(Z)\right|\right\}. \tag{16}$$

where $W=[w_1,\cdots,w_s]^{\mathrm{T}}\in\mathbb{R}^s$ where $s>1$ is network node number; $Z\in\Omega_Z\subset\mathbb{R}^n$ is the network input; and $\Xi(X)\in\mathbb{R}^s$ expresses the Gaussian function with $\Xi_i(Z)$ being $\Xi_i(Z)=\exp\big(-(Z-\varsigma_i)^{\mathrm{T}}(Z-\varsigma_i)/\nu_i^2\big)$, where $\varsigma_i=[\varsigma_{i1},\cdots,\varsigma_{in}]^{\mathrm{T}}\in\mathbb{R}^n$ and ν_i are the center and width of $\Xi_i(Z)$. Before proceeding further, the estimation of θ^* is defined as $\hat{\theta}$, while the estimation error $\tilde{\theta}$ is denoted as $\tilde{\theta}=\theta^*-\hat{\theta}$. We provide an important analysis, as

$$\begin{aligned}f(Z)\leq&\begin{bmatrix}\bar{W}\\ \bar{\zeta}\end{bmatrix}^{\mathrm{T}}\begin{bmatrix}\Xi(Z)\\ 1\end{bmatrix}\leq\left\|\begin{bmatrix}\bar{W}\\ \bar{\zeta}\end{bmatrix}^{\mathrm{T}}\right\|\left\|\begin{bmatrix}\Xi(Z)\\ 1\end{bmatrix}\right\|\\ =&\bar{W}\|\Xi(Z)\|+\bar{\zeta}\leq\theta^*\Psi(Z)\end{aligned} \tag{17}$$

wherein $\theta^*\geq\max\{\bar{W},\bar{\zeta}\}$ and $\Psi(Z)=1+\|\Xi(Z)\|>0$ are a virtual parameter and a computable scalar function. In particular, this study just needs to adjust one parameter rather than each element of W^*, thus the number of adaptive parameters is greatly decreased.

III. Main Results

A. NN State Observer Design

First, the system dynamics (1) is rearranged by

$$\begin{cases}\dot{x}=Ax+Ky+\sum_{i=1}^{n}B_ig_iF_i\big(\bar{x}_i|\theta_i^*\big)+B_ng_n\tau\\ y=Cx\end{cases} \tag{18}$$

where $C=[1,\ldots,0,\ldots,0]^{\mathrm{T}}$, $B_i=[\underbrace{0,\ldots,0}_{i-1},1,0,\ldots,0]^{\mathrm{T}}$, $x=[x_1,\ldots,x_n]^{\mathrm{T}}$, $B_n=[0,\ldots,1]^{\mathrm{T}}$, $K=[k_1,\ldots,k_n]^{\mathrm{T}}$, and $A=\begin{bmatrix}-k_1 & & & \\ \vdots & & I_{n-1} & \\ -k_n & 0 & \cdots & 0\end{bmatrix}$ is the Hurwitz matrix. Thus, for any symmetric positive-definite matrix N, there exists a matrix M such that $A^{\mathrm{T}}N+NA=-M$.

Construct the following NN state observer, as

$$\begin{cases}\dot{\hat{x}}=A\hat{x}+Ky+\sum_{i=1}^{n}B_ig_i\hat{F}_i(\hat{\bar{x}}_i|\bar{\theta})+B_ng_n\tau\\ \hat{y}=C\hat{x}\end{cases}. \tag{19}$$

Let the state observation error $\tilde{x}$ as $\tilde{x}=x-\hat{x}=[x_1-\hat{x}_1,\ldots,x_n-\hat{x}_n]^{\mathrm{T}}$. Then, by combining (18)-(19), one has

$$\dot{\tilde{x}}=A\tilde{x}+\sum_{i=1}^{n}B_ig_i\big(F_i(\bar{x}_i|\theta_i^*)-\hat{F}_i(\hat{\bar{x}}_i|\bar{\theta})\big) \tag{20}$$

where $\bar{\theta}=\max\{\theta_1^{*2},\cdots,\theta_n^{*2}\}$ and its estimation is $\hat{\theta}$, while the estimation error is denoted as $\tilde{\theta}=\bar{\theta}-\hat{\theta}$.

Select the Lyapunov function V_0 about the estimation error $\tilde{x}$ as $V_0=\tilde{x}^{\mathrm{T}}N\tilde{x}$, and then its derivative is calculated by

$$\begin{aligned}\dot{V}_0=&-\Big(A\tilde{x}+\sum_{i=1}^{n}B_ig_i\Big(F_i(\bar{x}_i|\theta_i^*)-\hat{F}_i(\hat{\bar{x}}_i|\bar{\theta})\Big)\Big)^{\mathrm{T}}N\tilde{x}\\ &+\tilde{x}^{\mathrm{T}}N\Big(A\tilde{x}+\sum_{i=1}^{n}B_ig_i\Big(F_i(\bar{x}_i|\theta_i^*)-\hat{F}_i(\hat{\bar{x}}_i|\bar{\theta})\Big)\Big)\\ =&\tilde{x}^{\mathrm{T}}(AN^{\mathrm{T}}+NA)\tilde{x}+2\tilde{x}^{\mathrm{T}}N\sum_{i=1}^{n}B_ig_i\tilde{\theta}\Psi_i\\ \leq&-\lambda_{\min}(M)\|\tilde{x}\|^2+2\|\tilde{x}\|\|N\|\bar{g}\bar{\Psi}|\tilde{\theta}|.\end{aligned} \tag{21}$$

where $\bar{\Psi}=\max\{\Psi_1,\ldots,\Psi_n\}$.

Utilizing Young's inequality, results in

$$2\|\tilde{x}\|N\bar{g}\bar{\Psi}|\tilde{\theta}|\leq\|\tilde{x}\|^2+\Phi\tilde{\theta}^2 \tag{22}$$

where $\Phi=\bar{g}^2\|N\|^2\|\bar{\Psi}\|$.

By substituting (22) into (21), it follows that

$$\dot{V}_0\leq-\big(\lambda_{\min}(N)-1\big)\|\tilde{x}\|^2+\Phi\tilde{\theta}^2. \tag{23}$$

as long as $\lambda_{\min}(N)-1>0$, the estimation error converges to the bounded region. It should be noticed that the o(23) is an intermediate process where the term $\Phi\tilde{\theta}^2$ will be solved in the controller design.

B. Controller Design

First, the tracking errors are denoted as

$$z_1=\hat{x}_1-y_d,\quad z_i=\hat{x}_i-\varpi_i,\quad i=2,\cdots,n \tag{24}$$

where ϖ_i is the the FTCF's output with a virtual input α_{i-1}. To evade recursive differentiation, a FTCF is constructed as

$$\begin{aligned}\dot{\vartheta}_{j,1} =& -L_1|\vartheta_{j,1}-\alpha_j|^{\frac{1}{2}}\mathrm{sign}(\vartheta_{i,1}-\alpha_i)+\vartheta_{i,2}\\ \dot{\vartheta}_{j,2} =& -L_2\mathrm{sign}(\vartheta_{j,2}-\dot{\vartheta}_{j,1}),\ j=1,\cdots,n-1\end{aligned} \tag{25}$$

where ϖ_j can be approximated by $\vartheta_{j,1}$, i.e., $\varpi_j=\vartheta_{j,1}$.

To the filtering error, a filtering–error compensation system is proposed as

$$\begin{aligned}\dot{\upsilon}_i =& -c_i\upsilon_i+g_i(\varpi_{i+1}-\alpha_i)+g_i\upsilon_{i+1}-h_i\upsilon_i^b,\\ \dot{\upsilon}_n =& -c_n\upsilon_n-h_n\upsilon_n^b,\quad i=1,\cdots,n-1\end{aligned} \tag{26}$$

where $\upsilon_i(0)=0$, $\upsilon_n(0)=0$, g_i, c_i, h_i, c_n, and h_n are positive constants, and the parameter b holds $\frac{1}{2}<b=\frac{b_1}{b_2}<1$ with

b_1 and b_2 being positive odd integers. Define the compensated error signals as

$$s_i = z_i - \upsilon_i,\ i = 1, \ldots, n \tag{27}$$

Step 1: Based on (1) and (27), we obtain

$$\dot{s}_1 = g_1\alpha_1 + g_1(\varpi_2 - \alpha_1) + g_1 z_2 + F_1 - \dot{y}_d - \dot{\upsilon}_1. \tag{28}$$

To avoid the differentiation of α_1, the FTCF is applied as

$$\begin{aligned}\dot{\vartheta}_{1,1} =& -L_1|\vartheta_{1,1} - \alpha_1|^{\frac{1}{2}}\text{sign}(\vartheta_{1,1} - \alpha_1) + \vartheta_{1,2}\\ \dot{\vartheta}_{1,2} =& -L_2\text{sign}(\vartheta_{1,2} - \dot{\vartheta}_{1,1})\end{aligned} \tag{29}$$

where α_1 and $\varpi_2 = \vartheta_{1,1}$ can be viewed as the input and output signals of the FTCF, and $\vartheta_{1,1}(0) = 0$ and $\vartheta_{1,2}(0) = 0$.

The RBFNN is adopted to cope with the nonlinear function F_1, and then we recall (17) to get the result, as

$$F_1 \leq \bar{W}_1\|\Xi_1(Z_1)\| + \bar{\zeta}_1 \leq \theta_1^*\Psi_1 \tag{30}$$

where $Z_1 = [\hat{x}_1, y_d, \dot{y}_d]^{\mathrm{T}}$ is the RBFNN's input, $\theta_1^* \geq \max\{\bar{W}_1, \bar{\zeta}_1\}$ and $\Psi_1 = 1 + \|\Xi_1(Z)\|$.

We define compact set $\Omega_z : \{|s_i| < k_{di}\}$, where $k_{di} > 0$ is a prespecified constant. Then, we select the following BLF, which grows to infinity whenever s_1 closes to k_{d1}, as

$$V_1 = \frac{1}{2}\log\frac{k_{d1}^2}{k_{d1}^2 - s_1^2} + \frac{1}{2}\upsilon_1^2 \tag{31}$$

where $k_{d1} > 0$. Next, the time derivative of V_1 along (26), (28) and (30) can be derived by

$$\begin{aligned}\dot{V}_1 \leq& \frac{s_1^2}{2p_1^2\big(k_{d1}^2 - s_1^2\big)^2}\theta_1^{*2}\Psi_1^2 + \frac{1}{2}p_1^2 + \frac{s_1}{k_{d1}^2 - s_1^2}\Big(g_1\alpha_1 - \dot{y}_d\\ &+ g_1(\varpi_2 - \alpha_1) + g_1 z_2 - \dot{\upsilon}_1\Big) + g_1(\varpi_2 - \alpha_1)\upsilon_1 - c_1\upsilon_1^2\\ &+ g_1\upsilon_1\upsilon_2 - h_1\upsilon_1^{b+1}.\end{aligned} \tag{32}$$

From Lemma 5 and Assumption 2, one knows that $|\varpi_1 - \alpha_1| \leq \chi_1$ can be guaranteed after finite time T_1 and $|g_1| \leq \bar{g}$. Then, we apply the Young's inequality to get the following:

$$g_1\upsilon_1\upsilon_2 \leq \frac{1}{2}\bar{g}\upsilon_1^2 + \frac{1}{2}\bar{g}\upsilon_2^2, \tag{33a}$$

$$g_1(\varpi_2 - \alpha_1)\upsilon_1 \leq \frac{1}{2}\frac{\bar{g}}{\sigma_1}\upsilon_1^2 + \frac{1}{2}\bar{g}\sigma_1\chi_1^2. \tag{33b}$$

where σ_1 is a positive scalar.

Integrating (33) into (32) yields

$$\begin{aligned}\dot{V}_1 \leq& \frac{s_1^2}{2p_1^2\big(k_{d1}^2 - s_1^2\big)^2}\theta_1^{*2}\Psi_1^2 + \frac{1}{2}p_1^2 + \frac{s_1}{k_{d1}^2 - s_1^2}\Big(g_1\alpha_1\\ &+ g_1(\varpi_2 - \alpha_1) + g_1 z_2 - \dot{y}_d - \dot{\upsilon}_1\Big) + \frac{\bar{g}\sigma_1\chi_1^2}{2}\\ &- \left(c_1 - \frac{\bar{g}_1}{2} - \frac{\bar{g}}{2\sigma_1}\right)\upsilon_1^2 + \frac{\bar{g}_1}{2}\upsilon_2^2 - h_1\upsilon_1^{b+1}.\end{aligned} \tag{34}$$

To guarantee the system stability, a virtual control input α_1 is designed as

$$\begin{aligned}\alpha_1 = \frac{1}{g_1}\Bigg(& -q_1 z_1 - \frac{1}{2p_1^2}\frac{s_1}{k_{d1}^2 - s_1^2}\hat{\theta}_1\Psi_1^2 - \Big(\frac{s_1}{k_{d1}^2 - s_1^2}\Big)^{\frac{b-1}{2}}\\ &\times \beta_1 s_1^{\frac{b+1}{2}} + \dot{y}_d - \frac{h_1}{b+1}\Big(\frac{s_1}{k_{d1}^2 - s_1^2}\Big)^b\Bigg)\end{aligned} \tag{35}$$

where $p_1 > 0$, $q_1 > 0$ and $\beta_1 > 0$ are design constants.

Substituting (35) and the first equation of (26) into (34) leads to the following result:

$$\begin{aligned}\dot{V}_1 \leq& \frac{s_1}{k_{d1}^2 - s_1^2}g_1 s_2 - \frac{s_1}{k_{d1}^2 - s_1^2}q_1 s_1 - \beta_1\Big(\frac{s_1}{k_{d1}^2 - s_1^2}\Big)^{\frac{b+1}{2}}\\ &\times s_1^{\frac{b+1}{2}} - \frac{h_1}{b+1}\Big(\frac{s_1}{k_{d1}^2 - s_1^2}\Big)^{b+1} + h_1\frac{s_1}{k_{d1}^2 - s_1^2}\upsilon_1^b\\ &+ \frac{\Psi_1^2}{2p_1^2}\frac{s_1^2}{\big(k_{d1}^2 - s_1^2\big)^2}\Big(\theta_1^{*2} - \hat{\theta}_1\Big) + \frac{1}{2}p_1^2 - \Bigg(c_1 - \frac{\bar{g}}{2}\\ &- \frac{\bar{g}}{2\sigma_1}\Bigg)\upsilon_1^2 + \frac{\bar{g}}{2}\upsilon_2^2 + \frac{\bar{g}\sigma_1\chi_1^2}{2} - h_1\upsilon_1^{b+1}.\end{aligned} \tag{36}$$

By recalling Lemma 3, one arrives at

$$h_1\frac{s_1}{k_{d1}^2 - s_1^2}\upsilon_1^b \leq \frac{h_1}{b+1}\Big(\frac{s_1}{k_{d1}^2 - s_1^2}\Big)^{b+1} + \frac{h_1 b}{b+1}\upsilon_1^{b+1}. \tag{37}$$

Along with (36) and (37), one can deduce that

$$\begin{aligned}\dot{V}_1 \leq& \frac{s_1}{k_{d1}^2 - s_1^2}g_1 s_2 - \frac{s_1}{k_{d1}^2 - s_1^2}q_1 s_1 - \beta_1\Big(\frac{s_1}{k_{d1}^2 - s_1^2}\Big)^{\frac{b+1}{2}}\\ &\times s_1^{\frac{b+1}{2}} - \frac{h_1}{b+1}\upsilon_1^{b+1} + \frac{h_1}{b+1}\Big(\frac{s_1}{k_{d1}^2 - s_1^2}\Big)^{b+1} + \frac{\Psi_1^2}{2p_1^2}\\ &\times \frac{s_1^2}{\big(k_{d1}^2 - s_1^2\big)^2}\Big(\theta_1^{*2} - \hat{\theta}_1\Big) + \frac{1}{2}p_1^2 - \left(c_1 - \frac{\bar{g}}{2} - \frac{\bar{g}}{2\sigma_1}\right)\\ &\times \upsilon_1^2 + \frac{\bar{g}}{2}\upsilon_2^2 + \frac{\bar{g}\sigma_1\chi_1^2}{2}.\end{aligned} \tag{38}$$

Step i *($i = 2, \cdots, n-1$):* The derivative of the error compensation signal $s_i = z_i - \upsilon_i$ can be given by

$$\begin{aligned}\dot{s}_i =& g_i x_{i+1} + F_i - \dot{\alpha}_i - \dot{\upsilon}_i\\ =& g_i\alpha_i + g_i(\varpi_{i+1} - \alpha_i) + g_i z_{i+1} + F_i - \dot{\varpi}_i - \dot{\upsilon}_i.\end{aligned} \tag{39}$$

To address the problem of exponential explosion, we adopt the following FTCT via Lemma 5, as

$$\begin{aligned}\dot{\vartheta}_{i,1} =& -L_1|\vartheta_{i,1} - \alpha_i|^{\frac{1}{2}}\text{sign}(\vartheta_{i,1} - \alpha_i) + \vartheta_{i,2}\\ \dot{\vartheta}_{i,2} =& -L_2\text{sign}(\vartheta_{i,2} - \dot{\vartheta}_{i,1})\end{aligned} \tag{40}$$

where α_{i+1} and $\varpi_i = \vartheta_{i,1}$ can be regarded as the input and output signals of the FTCF, respectively; and $\vartheta_{i,1}(0) = 0$ and $\vartheta_{i,2}(0) = 0$.

Similarly, we apply the RBFNN to deal with F_i in (39), as

$$F_i \leq \bar{W}_i\|\Xi_i(Z_i)\| + \bar{\zeta}_i \leq \theta_i^*\Psi_i \tag{41}$$

where $Z_i = [\hat{x}_1, \ldots, \hat{x}_i, y_d, \dot{y}_d]^{\mathrm{T}}$, $\theta_i^* \geq \max\{\bar{W}_i, \bar{\zeta}_i\}$ and $\Psi_i = 1 + \|\Xi_i\| > 0$.

Define the composite BLF for the $i-$th subsystem, as

$$V_i = V_{i-1} + \frac{1}{2}\log\frac{k_{di}^2}{k_{di}^2 - s_i^2} + \frac{1}{2}\upsilon_i^2 \tag{42}$$

where $k_{di} > 0$ stands for a prespecified constant. Taking the derivative of (42) along (39) and (41) yields

$$\begin{aligned}\dot{V}_i =&\dot{V}_{i-1} + \frac{s_i}{k_{di}^2 - s_i^2}\Big(g_i\alpha_i + g_i(\varpi_{i+1} - \alpha_i) + g_i z_{i+1} \\ &+ F_i - \varpi_i - \dot{\upsilon}_i\Big) + g_i(\varpi_{i+1} - \alpha_i)\upsilon_i + g_i\upsilon_i\upsilon_{i+1} \\ &- c_i\upsilon_i^2 - h_i\upsilon_i^{b+1} \\ \leq&\dot{V}_{i-1} + \frac{s_i^2}{2p_i^2\big(k_{di}^2 - s_i^2\big)^2}\theta_i^{*2}\Psi_i^2 + \frac{1}{2}p_i^2 + \frac{s_i}{k_{di}^2 - s_i^2} \\ &\times\Big(g_i\alpha_i + g_i(\varpi_i - \alpha_i) + g_i z_{i+1} - \varpi_i - \dot{\upsilon}_i\Big) - c_i\upsilon_i^2 \\ &+ g_i(\varpi_{i+1} - \alpha_i)\upsilon_i + g_i\upsilon_i\upsilon_{i+1} - h_i\upsilon_i^{b+1}. \end{aligned} \tag{43}$$

Based on Lemma 5 and Assumption 2, one can get a conclusion that $|\varpi_i - \alpha_i| \leq \chi_i$ is achieved after finite time T_i and $|g_i| \leq \bar{g}_i$. Then, we have

$$g_i\upsilon_i\upsilon_{i+1} \leq \frac{1}{2}\bar{g}\upsilon_i^2 + \frac{1}{2}\bar{g}\upsilon_{i+1}^2, \tag{44a}$$

$$g_i(\varpi_{i+1} - \alpha_i)\upsilon_i \leq \frac{1}{2}\frac{\bar{g}}{\sigma_i}\upsilon_i^2 + \frac{1}{2}\bar{g}\sigma_i\chi_i^2. \tag{44b}$$

where ρ_i is a positive scalar.

Then, by inserting (44) into (43), one gets

$$\begin{aligned}\dot{V}_i \leq&\dot{V}_{i-1} + \frac{s_i^2}{2p_i^2\big(k_{di}^2 - s_i^2\big)^2}\theta_i^{*2}\Psi_i^2 + \frac{1}{2}p_i^2 + \frac{s_i}{k_{di}^2 - s_i^2} \\ &\times\big(g_i\alpha_i + g_i(\varpi_i - \alpha_i) + g_i z_{i+1} - \varpi_i - \dot{\upsilon}_i\big) + \frac{\bar{g}}{2}\upsilon_n^2 \\ &- \left(c_i - \frac{\bar{g}}{2} - \frac{\bar{g}}{2\sigma_i}\right)\upsilon_i^2 + \frac{\bar{g}\sigma_i\chi_i^2}{2} - h_i\upsilon_i^{b+1}. \end{aligned} \tag{45}$$

As in *Step 1*, we design the virtual input α_2, as follows:

$$\begin{aligned}\alpha_i =&\frac{1}{g_i}\bigg(-\frac{1}{2p_i^2}\frac{s_i}{k_{di}^2 - s_i^2}\hat{\theta}_i\Psi_i^2 - \Big(\frac{s_i}{k_{di}^2 - s_i^2}\Big)^{\frac{b-1}{2}}\beta_i s_i^{\frac{b+1}{2}} + \dot{\varpi}_i \\ &- q_i z_i - \frac{h_i}{b+1}\Big(\frac{s_i}{k_{di}^2 - s_i^2}\Big)^b - \frac{s_j g_j(k_{di}^2 - s_i^2)}{(k_{dj}^2 - s_j^2)}\bigg) \end{aligned} \tag{46}$$

where $j = i - 1$, and $p_i > 0$, $q_i > 0$ and $\beta_i > 0$.

By invoking (38), (43)–(46), it can be readily obtained that

$$\begin{aligned}\dot{V}_i \leq&\dot{V}_{i-1} + \frac{s_i}{k_{di}^2 - s_i^2}g_i s_{i+1} - \frac{s_i}{k_{di}^2 - s_i^2}q_i s_i - \beta_i s_i^{\frac{b+1}{2}} \\ &\times\Big(\frac{s_i}{k_{di}^2 - s_i^2}\Big)^{\frac{b+1}{2}} - \frac{h_i}{b+1}\upsilon_i^{b+1} - g_j\frac{s_j}{k_{dj}^2 - s_j^2}s_j^b \\ &+ \frac{\Psi_i^2}{2p_i^2}\frac{s_i^2}{\big(k_{di}^2 - s_i^2\big)^2}\Big(\theta_i^{*2} - \hat{\theta}_i\Big) - \Big(c_i - \bar{g} - \frac{\bar{g}}{2\sigma_i}\Big)\upsilon_i^2 \\ &+ \frac{1}{2}p_i^2 + \frac{\bar{g}}{2}\upsilon_n^2 + \frac{\bar{g}\sigma_i\chi_i^2}{2}. \end{aligned} \tag{47}$$

Step n: For the last step, it goal is to focus on designing an actual control law u. The derivative of the error compensation signal $s_n = z_n - \upsilon_n$ with respect to time is calculated by

$$\dot{s}_n = g_n\,\mathrm{sat}(u) + F_n - \dot{\varpi}_n - \dot{\upsilon}_n. \tag{48}$$

By utilizing the RBFNN to approximate F_n in (48), it follows

$$F_n \leq \bar{W}_n\|\Xi_n(Z_n)\| + \bar{\zeta}_n \leq \theta_n^*\Psi_n \tag{49}$$

where $Z_n = [\hat{x}_1, \ldots, \hat{x}_n, y_d, \dot{y}_d]^{\mathrm{T}}$, $\theta_n^* \geq \max\{\bar{W}_n, \bar{\zeta}_n\}$ and $\Psi_n = 1 + \|\Xi_n\|$ are the virtual parameter and computable scalar function, respectively.

To compensate for the saturation-approximation error, an ACS is constructed as

$$\dot{\zeta} = -\eta_1\zeta - \eta_2\zeta^b - \frac{\big(1 + \Xi(\zeta)\big)\Big(\big(\frac{s_n}{k_{dn}^2 - s_n^2}\big)^2 + \Delta u^2\Big)}{2\zeta^2}\zeta + \Delta u \tag{50}$$

where $\Xi(\zeta)$ is a smooth and nonsingular function, as

$$\Xi(\zeta) = \begin{cases} 0, & \text{if } |\zeta| \leq \iota_a \\ 1, & \text{if } |\zeta| \geq \iota_b \\ 1 - \cos\left(\frac{\pi}{2}\sin\left(\frac{\pi}{2}\frac{\zeta^2 - \iota_a}{\iota_b - \iota_a}\right)\right), & \text{otherwise} \end{cases} \tag{51}$$

where $\iota_a > 0$ and $\iota_b > 0$ are arbitrarily design constants, ζ is an auxiliary dynamic variable, $\Delta u = \mathrm{sat}(u) - \kappa u$, $\eta_1 > 1$ and $\eta_2 > 0$ are design constants, and the term $\eta_2\zeta^b$ in (50) can guarantee the fast finite-time stability of the ACS.

Consider the composite BLF for the last subsystem, as

$$V_n = V_{n-1} + \frac{1}{2}\log\frac{k_{dn}^2}{k_{dn}^2 - s_n^2} + \frac{1}{2}\upsilon_n^2 + \frac{1}{2}\zeta^2 \tag{52}$$

where k_{dn} is a positive prespecified constant.

Case 1: For $|\zeta| \leq \iota_a$, it means that $\dot{\zeta} = -\eta_1\zeta - \eta_2\zeta^b - \frac{\big(\frac{s_n}{k_{dn}^2 - s_n^2}\big)^2 + \Delta u^2}{2\zeta^2}\zeta + \Delta u$. By differentiating (52) along (48) and (49), one obtains

$$\begin{aligned}\dot{V}_n \leq&\dot{V}_{n-1} + \frac{s_n^2}{2p_n^2\big(k_{dn}^2 - s_n^2\big)^2}\theta_n^{*2}\Psi_n^2 + \frac{1}{2}p_n^2 + \frac{s_n}{k_{dn}^2 - s_n^2} \\ &\times\big(g_n u + F_n - \dot{\varpi}_n - \dot{\upsilon}_n\big) - c_n\upsilon_n^2 - h_n\upsilon_n^{b+1} - \eta_1\zeta^2 \\ &- \eta_2\zeta^{b+1} - \frac{1}{2}\Big(\frac{s_n}{k_{dn}^2 - s_n^2}\Big)^2 - \frac{1}{2}\Delta u^2 + \Delta u\zeta. \end{aligned} \tag{53}$$

From (53), we develop the following actual control law, as

$$\begin{aligned}u =&\frac{1}{g_n\kappa}\bigg(-q_n z_n - \frac{1}{2p_n^2}\frac{s_n}{k_{dn}^2 - s_n^2}\hat{\theta}_n\Psi_n^2 + \dot{\varpi}_n - \beta_n s_n^{\frac{b+1}{2}} \\ &\times\Big(\frac{s_n}{k_{dn}^2 - s_n^2}\Big)^{\frac{b-1}{2}} - \frac{h_n}{b+1}\Big(\frac{s_n}{k_{dn}^2 - s_n^2}\Big)^b \\ &- \frac{s_m g_m(k_{dn}^2 - s_n^2)}{(k_{dm}^2 - s_m^2)} + \zeta\bigg) \end{aligned} \tag{54}$$

where $m = n - 1$, and $p_n > 0$, $q_n > 0$ and $\beta_n > 0$ stand for design constants.

Applying the Young's inequality leads to

$$\Delta u\zeta \leq \frac{1}{2}\Delta u^2 + \frac{1}{2}\zeta^2, \tag{55a}$$

$$\frac{s_n}{k_{dn}^2 - s_n^2}\zeta \leq \frac{1}{2}\Big(\frac{s_n^2}{k_{dn}^2 - s_n^2}\Big)^2 + \frac{1}{2}\zeta^2. \tag{55b}$$

Using Lemma 4 and substituting (54) and (55) into (53) yield

$$\dot{V}_n \leq -\sum_{i=1}^{n}\frac{s_i}{k_{di}^2-s_i^2}q_i s_i-\sum_{i=1}^{n}\beta_i\Big(\frac{s_i}{k_{di}^2-s_i^2}\Big)^{\frac{b+1}{2}}s_i^{\frac{b+1}{2}} -\sum_{i=1}^{n}\frac{h_i}{b+1}\upsilon_i^{b+1}+\sum_{i=1}^{n}\frac{1}{2p_i^2}-\sum_{i=1}^{n}\Gamma\upsilon_i^2-(\eta_1-1)\zeta^2 +\sum_{i=1}^{n}\frac{1}{2p_i^2}\frac{s_i^2}{\big(k_{di}^2-s_i^2\big)^2}\Psi_i^2\big(\theta_i^{*2}-\hat{\theta}_i\big)-\eta_2\zeta^{b+1}+\Delta \quad (56)$$

where $\Gamma=\min\big\{c_1-\frac{\bar{g}}{2}-\frac{\bar{g}}{2\sigma_1},c_2-\bar{g}-\frac{\bar{g}}{2\sigma_2},\ldots,c_{n-1}-\bar{g}-\frac{\bar{g}}{2\sigma_{n-1}},c_n-\frac{\bar{g}}{2}\big\}$ with $c_1>\frac{\bar{g}}{2}+\frac{\bar{g}}{2\sigma_1}$, $c_2>\bar{g}+\frac{\bar{g}}{2\sigma_2}$, $c_{n-1}>\bar{g}+\frac{\bar{g}}{2\sigma_{n-1}}$, and $c_n>\frac{\bar{g}}{2}$, and $\Delta=\frac{(n-1)\bar{g}}{2}\max\big\{\sigma_1\chi_1^2,\sigma_2\chi_2^2,\ldots,\sigma_{n-1}\chi_{n-1}^2\big\}$.

Case 2: For $|\zeta|\geq\iota_b$, it means that $\dot{\zeta}=-\eta_1\zeta-\eta_2\zeta^b-\frac{\big(\frac{s_n}{k_{dn}^2-s_n^2}\big)^2+\Delta u^2}{\zeta^2}\zeta+\Delta u$. Similar to (53), the derivative of (52) along (54) can be given by

$$\dot{V}_n \leq \dot{V}_{n-1}+\frac{s_n^2}{2p_n^2\big(k_{dn}^2-s_n^2\big)^2}\theta_n^{*2}\Psi_n^2+\frac{1}{2}p_n^2+\frac{s_n}{k_{dn}^2-s_n^2} \times\big(g_n u+F_n-\dot{\varpi}_n-\dot{\upsilon}_n\big)-c_n\upsilon_n^2-h_n\upsilon_n^{b+1}-\eta_1\zeta^2 -\eta_2\zeta^{b+1}-\Big(\frac{s_n}{k_{dn}^2-s_n^2}\Big)^2-\Delta u^2+\Delta u\zeta. \quad (57)$$

The following inequalities hold as

$$\Delta u\zeta\leq\Delta u^2+\frac{1}{4}\zeta^2, \quad (58a)$$

$$\frac{s_n}{k_{dn}^2-s_n^2}\zeta\leq\Big(\frac{s_n^2}{k_{dn}^2-s_n^2}\Big)^2+\frac{1}{4}\zeta^2. \quad (58b)$$

Bearing in mind (57) and (58), it can be deduced that

$$\dot{V}_n \leq -\sum_{i=1}^{n}\frac{s_i}{k_{di}^2-s_i^2}q_i s_i-\sum_{i=1}^{n}\beta_i\Big(\frac{s_i}{k_{di}^2-s_i^2}\Big)^{\frac{b+1}{2}}s_i^{\frac{b+1}{2}} -\sum_{i=1}^{n}\frac{h_i}{b+1}\upsilon_i^{b+1}+\sum_{i=1}^{n}\frac{1}{2p_i^2}-\sum_{i=1}^{n}\Gamma\upsilon_i^2-\Big(\eta_1-\frac{1}{2}\Big)\zeta^2 +\sum_{i=1}^{n}\frac{1}{2p_i^2}\frac{s_i^2}{\big(k_{di}^2-s_i^2\big)^2}\Psi_i^2\big(\theta_i^{*2}-\hat{\theta}_i\big)-\eta_2\zeta^{b+1}+\Delta \quad (59)$$

Case 3: For the remaining case, it has $1+\Xi(\zeta)\in(1,2)$. In what follows, we can obtain

$$\dot{V}_n \leq \dot{V}_{n-1}+\frac{s_n^2}{2p_n^2\big(k_{dn}^2-s_n^2\big)^2}\theta_n^{*2}\Psi_n^2+\frac{1}{2}p_n^2+\frac{s_n}{k_{dn}^2-s_n^2} \times\big(g_n u+F_n-\dot{\varpi}_n-\dot{\upsilon}_n\big)-c_n\upsilon_n^2-h_n\upsilon_n^{b+1}-\eta_1\zeta^2 -\eta_2\zeta^{b+1}-\frac{\big(1+\Xi(\zeta)\big)}{2}\Big(\frac{s_n}{k_{dn}^2-s_n^2}\Big)^2-\frac{\big(1+\Xi(\zeta)\big)}{2} \times\Delta u^2+\Delta u\zeta. \quad (60)$$

According to the Young's inequality, it is true that

$$\Delta u\zeta\leq\frac{\big(1+\Xi(\zeta)\big)}{2}\Delta u^2+\frac{1}{2\big(1+\Xi(\zeta)\big)}\zeta^2, \quad (61a)$$

$$\frac{s_n}{k_{dn}^2-s_n^2}\zeta\leq\frac{\big(1+\Xi(\zeta)\big)}{2}\Big(\frac{s_n^2}{k_{dn}^2-s_n^2}\Big)^2+\frac{1}{2\big(1+\Xi(\zeta)\big)}\zeta^2. \quad (61b)$$

Recalling Lemma 4 and combining (60) and (61), one has

$$\dot{V}_n \leq -\sum_{i=1}^{n}\frac{s_i}{k_{di}^2-s_i^2}q_i s_i-\sum_{i=1}^{n}\beta_i\Big(\frac{s_i}{k_{di}^2-s_i^2}\Big)^{\frac{b+1}{2}}s_i^{\frac{b+1}{2}} -\sum_{i=1}^{n}\frac{h_i}{b+1}\upsilon_i^{b+1}+\sum_{i=1}^{n}\frac{1}{2p_i^2}-\Big(\eta_1-\frac{1}{\big(1+\Xi(\zeta)\big)}\Big) \times\zeta^2-\sum_{i=1}^{n}\Gamma\upsilon_i^2+\sum_{i=1}^{n}\frac{1}{2p_i^2}\frac{s_i^2}{\big(k_{di}^2-s_i^2\big)^2}\Psi_i^2\big(\theta_i^{*2}-\hat{\theta}_i\big) -\eta_2\zeta^{b+1}+\Delta. \quad (62)$$

Let a variable as $\bar{\theta}=\max\big\{\theta_1^{*2},\ldots,\theta_n^{*2}\big\}$ and its estimation is denoted as $\hat{\theta}$. The adaptive parameter $\hat{\theta}$ is updated by

$$\dot{\hat{\theta}}=\sum_{i=1}^{n}\frac{\gamma}{2p_i^2}\frac{s_i^2}{\big(k_{di}^2-s_i^2\big)^2}\Psi_i^2-2\gamma\rho\hat{\theta} \quad (63)$$

where γ and ρ are positive design constants. Accordingly, in (35), (46) and (54), the estimated values $\hat{\theta}_1$, $\hat{\theta}_i$ and $\hat{\theta}_n$ are uniformity represented by $\hat{\theta}$ in (63). As a result, the actual control law can be rewritten by the following form:

$$u=\frac{1}{g_n\kappa}\Big(-q_n z_n-\frac{1}{2p_n^2}\frac{s_n}{k_{dn}^2-s_n^2}\hat{\theta}_n\Psi_n^2+\dot{\varpi}_n-\beta_n s_n^{\frac{b+1}{2}} \times\Big(\frac{s_n}{k_{dn}^2-s_n^2}\Big)^{\frac{b-1}{2}}-\frac{h_n}{b+1}\Big(\frac{s_n}{k_{dn}^2-s_n^2}\Big)^b -\frac{s_m g_m(k_{dn}^2-s_n^2)}{(k_{dm}^2-s_m^2)}+\zeta\Big). \quad (64)$$

For readability, the mathematical parameters and the control algorithm are shown in Table I and Algorithm 1, respectively.

C. Stability Analysis

Theorem 1: Consider a constrained nonlinear system (1), this study presents an observer-based adaptive finite-time neural controller of the actual control law in (64), virtual control laws in (35) and (46), adaptive law in (63), FTCTs in (29) and (40), and ACS in (50) and (51) that can guarantee i) the tracking errors converge to the bounded regions around the origin in finite time; ii) the full-state constraints are never violated.

Proof: i) Consider the estimation error $\tilde{\theta}=\bar{\theta}-\hat{\theta}$, we choose the composite Lyapunov function, as

$$V=V_0+V_n+\frac{1}{2\gamma}\tilde{\theta}^2 \quad (65)$$

Case 1: For $|\zeta|\leq\iota_a$, taking the derivative of (65) along (23), (56) and (63) gives

$$\dot{V}\leq-\frac{\big(\lambda_{\min}(N)-1\big)}{\lambda_{\max}(N)}\lambda_{\max}(N)\|\tilde{x}\|^2-\sum_{i=1}^{n}\frac{s_i}{k_{di}^2-s_i^2}q_i s_i+\Phi\tilde{\theta}^2 -\varrho\big(\lambda_{\max}(N)\|\tilde{x}\|^2\big)^{\frac{b+1}{2}}+\varrho\big(\lambda_{\max}(N)\|\tilde{x}\|^2\big)^{\frac{b+1}{2}}+2\rho\tilde{\theta}\hat{\theta} -\sum_{i=1}^{n}\beta_i\Big(\frac{s_i}{k_{di}^2-s_i^2}\Big)^{\frac{b+1}{2}}s_i^{\frac{b+1}{2}}-\sum_{i=1}^{n}\frac{h_i}{b+1}\upsilon_i^{b+1}+\sum_{i=1}^{n}\frac{1}{2p_i^2} -\sum_{i=1}^{n}\Gamma\upsilon_i^2-(\eta_1-1)\zeta^2-\eta_2\zeta^{b+1}+\Delta \quad (66)$$

TABLE I
MATHEMATICAL PARAMETERS

1:	Desired signal and its derivative: y_d, $\dot{y}_d$.
2:	State observer and its parameters: $\hat{x}$, and k_i, $(i = 1, \ldots, n)$.
3:	Actual control input and its parameters: u, and q_n, p_n, β_n, h_n.
4:	Virtual control inputs and their parameters: α_1, α_i and α_n, and q_1, q_i, p_1, p_i, h_1, h_i, β_1, β_i, g_1, g_i, b $(i = 1, \ldots, n-1)$.
5:	Command filter signals and their parameters: ϖ_2 and ϖ_{i+1}, and L_1 and L_2, $(i = 1, \ldots, n-1)$.
6:	Filtering-error compensation signals and their parameters: υ_1, υ_i and υ_n, and c_1, c_i, c_n, h_1, h_i and h_n $(i = 1, \ldots, n-1)$.
7:	Improved Gaussian function and its parameters: φ_1 and φ_2.
8:	ACS signal and its parameters: ζ, and b, η_1, η_2, ι_a and ι_b.
9:	Adaptive law and its parameters: $\hat{\theta}$, and γ, p_i and ρ, $(i = 1, \ldots, n-1)$.

Algorithm 1: Design steps of the observer-based adaptive finite-time neural controller.

Input: desired signal y_d; unknown function f_i; external disturbance d_i; Gaussian function parameters φ_1 and φ_2; control parameters k_i, α_i, q_i, p_i, h_i, β_i, g_i, c_i, b, L_1, L_2, η_1, η_2, γ, ρ, η_1, and η_2; actuator saturation coefficients $\bar{u}_r$ and $\underline{u}_l$; sample time T and total sample step N.

while $i \leq N$ **do**

1. Apply the improved Gaussian function $h(u)$ and the ACS ζ;
2. Construct a NN state observer $\hat{x}$;
3. Select the composite Lyapunov function V_i;
4. Develop the FTCF $\vartheta_{i,1}$ and $\vartheta_{i,2}$ and the filtering-error compensation system υ_i;
5. Use the adaptive RBFNN to solve nonlinearities and disturbances;
6. Design the actual input u, virtual input α_i, and adaptive law $\hat{\theta}$.

end

Output: u, α_i, υ_i, $\hat{x}_i$, y, s_i, $\hat{\theta}$.

where N and η_1 are chosen to satisfy $\lambda_{\min}(N) - 1 > 0$ and $\eta_1 > 1$, respectively. It follows from the Yang's inequality that

$$\rho\tilde{\theta}\hat{\theta} = \rho\tilde{\theta}\bar{\theta} - \rho\tilde{\theta}\tilde{\theta} \leq -\frac{\rho(2\varsigma - 1)}{2\varsigma}\tilde{\theta}^2 + \frac{\rho\varsigma}{2}\bar{\theta}^2 \tag{67}$$

where $\varsigma > \frac{1}{2}$.

This together with (72) leads to

$$\begin{aligned}\dot{V} \leq & -\frac{\big(\lambda_{\min}(N) - 1\big)}{\lambda_{\max}(N)}\lambda_{\max}(N)\|\tilde{x}\|^2 - \sum_{i=1}^{n}\frac{s_i}{k_{di}^2 - s_i^2}q_i s_i \\ & - \varrho\big(\lambda_{\max}(N)\|\tilde{x}\|^2\big)^{\frac{b+1}{2}} + \varrho\big(\lambda_{\max}(N)\|\tilde{x}\|^2\big)^{\frac{b+1}{2}} \\ & - \sum_{i=1}^{n}\beta_i\Big(\frac{s_i}{k_{di}^2 - s_i^2}\Big)^{\frac{b+1}{2}} s_i^{\frac{b+1}{2}} - \sum_{i=1}^{n}\frac{h_i}{b+1}\upsilon_i^{b+1} + \sum_{i=1}^{n}\frac{1}{2p_i^2} \\ & - \sum_{i=1}^{n}\Gamma\upsilon_i^2 - (\eta_1 - 1)\zeta^2 - \eta_2\zeta^{b+1} + \Delta - \Big(\frac{2\mu}{\gamma} - \Phi\Big)\tilde{\theta}^2 \\ & - \Big(\frac{\mu}{\gamma}\tilde{\theta}^2\Big)^{\frac{b+1}{2}} + \Big(\frac{\mu}{\gamma}\tilde{\theta}^2\Big)^{\frac{b+1}{2}} + \rho\varsigma\bar{\theta}^2 \end{aligned} \tag{68}$$

where $\mu = \frac{\gamma\rho(2\varsigma-1)}{2\varsigma}$. Note that if $\frac{\mu}{\gamma}\tilde{\theta}^2 \geq 1$, one has $\big(\frac{\mu}{\gamma}\tilde{\theta}^2\big)^{\frac{b+1}{2}} - \frac{\mu}{\gamma}\tilde{\theta}^2 \leq \big(\frac{\mu}{\gamma}\big)\tilde{\theta}^2 - \big(\frac{\mu}{\gamma}\big)\tilde{\theta}^2 = 0$; else if $\frac{\mu}{\gamma}\tilde{\theta}^2 < 1$, one has $\big(\frac{\mu}{\gamma}\tilde{\theta}^2\big)^{\frac{b+1}{2}} - \frac{\mu}{\gamma}\tilde{\theta}^2 < 1 - \frac{\mu}{\gamma}\tilde{\theta}^2 < 1$. Therefore, whether $\frac{\mu}{\gamma}\tilde{\theta}^2 \geq 1$ or $\frac{\mu}{\gamma}\tilde{\theta}^2 < 1$, it follows that $\big(\frac{\mu}{\gamma}\tilde{\theta}^2\big)^{\frac{b+1}{2}} - \frac{\mu}{\gamma}\tilde{\theta}^2 < 1$.

Based on Lemma 3, the following conclusion satisfies:

$$\begin{aligned}\varrho\big(\lambda_{\max}(N)\|\tilde{x}\|^2\big)^{\frac{b+1}{2}} \leq & \ \varrho\lambda_{\max}(N)\|\tilde{x}\|^2 \\ & + \Big(\frac{1-b}{2}\Big)\Big(\frac{b+1}{2}\Big)^{\frac{1+b}{1-b}}. \end{aligned} \tag{69}$$

In what follows, combining (68) and (69) yields

$$\begin{aligned}\dot{V} \leq & -\Big(\frac{\big(\lambda_{\min}(N) - 1\big)}{\lambda_{\max}(N)} - \varrho\Big)\lambda_{\max}(N)\|\tilde{x}\|^2 - \sum_{i=1}^{n}\Big(\frac{s_i}{k_{di}^2 - s_i^2} \\ & \times q_i s_i\Big) - \varrho\big(\lambda_{\max}(N)\|\tilde{x}\|^2\big)^{\frac{b+1}{2}} - \sum_{i=1}^{n}\Big(\beta_i\Big(\frac{s_i}{k_{di}^2 - s_i^2}\Big)^{\frac{b+1}{2}} \\ & \times s_i^{\frac{b+1}{2}}\Big) - \sum_{i=1}^{n}\frac{h_i}{b+1}\upsilon_i^{b+1} + \sum_{i=1}^{n}\frac{1}{2p_i^2} - \sum_{i=1}^{n}\Gamma\upsilon_i^2 - \eta_2\zeta^{b+1} \\ & - (\eta_1 - 1)\zeta^2 + \Delta - \frac{\mu}{\gamma}\tilde{\theta}^2 - \Big(\frac{\mu}{\gamma}\tilde{\theta}^2\Big)^{\frac{b+1}{2}} + (1 + \rho\varsigma\bar{\theta}^2) \\ & + \Big(\frac{1-b}{2}\Big)\Big(\frac{b+1}{2}\Big)^{\frac{1+b}{1-b}}. \end{aligned} \tag{70}$$

By recalling Lemma 1 and (70), we can infer that

$$\begin{aligned}\dot{V} \leq & -\Big(\frac{\big(\lambda_{\min}(N) - 1\big)}{\lambda_{\max}(N)} - \varrho\Big)\lambda_{\max}(N)\|\tilde{x}\|^2 - \sum_{i=1}^{n}\Gamma\upsilon_i^2 \\ & - \varrho\big(\lambda_{\max}(N)\|\tilde{x}\|^2\big)^{\frac{b+1}{2}} - \sum_{i=1}^{n}q_i\log\frac{k_{di}^2}{k_{di}^2 - s_i^2} + \sum_{i=1}^{n}\frac{1}{2p_i^2} \\ & - \sum_{i=1}^{n}\beta_i\Big(\log\frac{k_{di}^2}{k_{di}^2 - s_i^2}\Big)^{\frac{b+1}{2}} - \sum_{i=1}^{n}\frac{h_i}{b+1}\upsilon_i^{b+1} - \eta_2\zeta^{b+1} \\ & - \Big(\frac{\mu}{\gamma}\tilde{\theta}^2\Big)^{\frac{b+1}{2}} - \frac{\mu}{\gamma}\tilde{\theta}^2 - (\eta_1 - 1)\zeta^2 + \Delta + (1 + \rho\varsigma\bar{\theta}^2) \\ & + \Big(\frac{1-b}{2}\Big)\Big(\frac{b+1}{2}\Big)^{\frac{1+b}{1-b}} \\ \leq & -\Lambda_1 V - \Lambda_2 V^{\frac{b+1}{2}} + \Lambda_3 \end{aligned} \tag{71}$$

where $\Lambda_1 = \min\big\{\frac{\lambda_{\min}(N)-1}{\lambda_{\max}(N)} - \varrho, 2q_i, 2\Gamma, 2\mu, 2(\eta_1 - 1)\big\}$, $\Lambda_2 = \min\big\{\varrho, \beta_i 2^{\frac{b+1}{2}}, \frac{h_i}{b+1}2^{\frac{b+1}{2}}, (2\mu)^{\frac{b+1}{2}}, \eta_2 2^{\frac{b+1}{2}}\big\}$, and $\Lambda_3 = \Delta + \big(1 + \rho\varsigma\bar{\theta}^2\big) + \big(\frac{1-b}{2}\big)\big(\frac{b+1}{2}\big)^{\frac{1+b}{1-b}} + \sum_{i=1}^{n}\frac{1}{2p_i^2}$.

Case 2: For $|\zeta| \leq \iota_a$, differentiating both sides of (65) becomes the following inequality:

$$\begin{aligned}\dot{V} \leq & -\frac{\big(\lambda_{\min}(N) - 1\big)}{\lambda_{\max}(N)}\lambda_{\max}(N)\|\tilde{x}\|^2 - \sum_{i=1}^{n}\frac{s_i}{k_{di}^2 - s_i^2}q_i s_i \\ & - \varrho\big(\lambda_{\max}(N)\|\tilde{x}\|^2\big)^{\frac{b+1}{2}} + \varrho\big(\lambda_{\max}(N)\|\tilde{x}\|^2\big)^{\frac{b+1}{2}} + 2\rho\tilde{\theta}\hat{\theta} \\ & - \sum_{i=1}^{n}\beta_i\Big(\frac{s_i}{k_{di}^2 - s_i^2}\Big)^{\frac{b+1}{2}} s_i^{\frac{b+1}{2}} - \sum_{i=1}^{n}\frac{h_i}{b+1}\upsilon_i^{b+1} + \sum_{i=1}^{n}\frac{1}{2p_i^2} \\ & - \sum_{i=1}^{n}\Gamma\upsilon_i^2 - \Big(\eta_1 - \frac{1}{2}\Big)\zeta^2 - \eta_2\zeta^{b+1} + \Delta. \end{aligned} \tag{72}$$

Similar calculation steps are made based on (67)-(70) to get

$$\begin{aligned}\dot{V} \leq & -\left(\frac{\big(\lambda_{\min}(N)-1\big)}{\lambda_{\max}(N)}-\varrho\right)\lambda_{\max}(N)\|\tilde{x}\|^2-\sum_{i=1}^{n}\Gamma\upsilon_i^2\\ & -\varrho\big(\lambda_{\max}(N)\|\tilde{x}\|^2\big)^{\frac{b+1}{2}}-\sum_{i=1}^{n}q_i\log\frac{k_{di}^2}{k_{di}^2-s_i^2}+\sum_{i=1}^{n}\frac{1}{2p_i^2}\\ & -\sum_{i=1}^{n}\beta_i\left(\log\frac{k_{di}^2}{k_{di}^2-s_i^2}\right)^{\frac{b+1}{2}}-\sum_{i=1}^{n}\frac{h_i}{b+1}\upsilon_i^{b+1}-\eta_2\zeta^{b+1}\\ & -\left(\frac{\mu}{\gamma}\tilde{\theta}^2\right)^{\frac{b+1}{2}}-\frac{\mu}{\gamma}\tilde{\theta}^2-\Big(\eta_1-\frac{1}{2}\Big)\zeta^2+\Delta+(1+\rho_\varsigma\bar{\theta}^2)\\ & +\left(\frac{1-b}{2}\right)\left(\frac{b+1}{2}\right)^{\frac{1+b}{1-b}}\\ \leq & -\Lambda_4 V-\Lambda_2 V^{\frac{b+1}{2}}+\Lambda_3 \end{aligned}\tag{73}$$

where $\eta_1 > \frac{1}{2}$ and $\Lambda_4 = \min\big\{\frac{\lambda_{\min}(N)-1}{\lambda_{\max}(N)} - \varrho, 2q_i, 2\Gamma, 2\mu, 2\big(\eta_1-\frac{1}{2}\big)\big\}$.

Case 3: For the remaining case, similar to the previous steps, the derivative of (65) along (62) is given by

$$\begin{aligned}\dot{V} \leq & -\frac{\big(\lambda_{\min}(N)-1\big)}{\lambda_{\max}(N)}\lambda_{\max}(N)\|\tilde{x}\|^2-\sum_{i=1}^{n}\frac{s_i}{k_{di}^2-s_i^2}q_i s_i\\ & -\varrho\big(\lambda_{\max}(N)\|\tilde{x}\|^2\big)^{\frac{b+1}{2}}+\varrho\big(\lambda_{\max}(N)\|\tilde{x}\|^2\big)^{\frac{b+1}{2}}+2\rho\tilde{\theta}\hat{\theta}\\ & -\sum_{i=1}^{n}\beta_i\Big(\frac{s_i}{k_{di}^2-s_i^2}\Big)^{\frac{b+1}{2}}s_i^{\frac{b+1}{2}}-\sum_{i=1}^{n}\frac{h_i}{b+1}\upsilon_i^{b+1}+\sum_{i=1}^{n}\frac{1}{2p_i^2}\\ & -\sum_{i=1}^{n}\Gamma\upsilon_i^2-\left(\eta_1-\frac{1}{\big(1+\Xi(\zeta)\big)}\right)\zeta^2-\eta_2\zeta^{b+1}+\Delta\\ \leq & -\Lambda_5 V-\Lambda_2 V^{\frac{b+1}{2}}+\Lambda_3 \end{aligned}\tag{74}$$

where $\eta_1 > 1/\big(1+\Xi(\zeta)\big)$ and $\Lambda_5 = \min\Big\{\frac{\lambda_{\min}(N)-1}{\lambda_{\max}(N)} - \varrho, 2q_i, 2\Gamma, 2\mu, 2\big(\eta_1-\frac{1}{1+\Xi(\zeta)}\big)\Big\}$.

According to the results of (71), (73) and (74), we have

$$\dot{V} \leq -\bar{\Lambda}V-\Lambda_2 V^{\frac{b+1}{2}}+\Lambda_3 \tag{75}$$

where $\bar{\Lambda}=\max\{\Lambda_1,\Lambda_4,\Lambda_5\}>1$. In view of Lemma 2, one knows that $V(x)$ approaches the bounded region as

$$\Omega=\left\{\lim_{t\to T}V\leq\min\left\{\frac{\Lambda_3}{(1-\iota_c)\bar{\Lambda}},\left(\frac{\Lambda_3}{(1-\iota_c)\Lambda_2}\right)^{\frac{2}{b+1}}\right\}\right\} \tag{76}$$

where $0<\iota_c<1$.

By computation, it follows from (65) and (76) that

$$\begin{aligned}&|\upsilon_i|\leq\min\left\{\sqrt{2\frac{\Lambda_3}{(1-\iota)\bar{\Lambda}}},\sqrt{2\left(\frac{\Lambda_3}{(1-\iota)\Lambda_2}\right)^{\frac{2}{b+1}}}\right\},\\ &|s_i|\leq\min\left\{k_{di}\sqrt{1-e^{-\frac{2\Lambda_3}{(1-\iota)\bar{\Lambda}}}},k_{di}\sqrt{1-e^{-2\left(\frac{\Lambda_3}{(1-\iota)\Lambda_2}\right)^{\frac{2}{b+1}}}}\right\}.\end{aligned}\tag{77}$$

From (27) and (77), the tracking error converges to the region

$$\begin{aligned}&|z_i|=|s_i+\upsilon_i|\leq|s_i|+|\upsilon_i|=\\ &\min\left\{\sqrt{2\frac{\Lambda_3}{(1-\iota_c)\Lambda_1}},\sqrt{2\left(\frac{\Lambda_3}{(1-\iota_c)\Lambda_2}\right)^{\frac{2}{b+1}}}\right\}+\\ &\min\left\{k_{di}\sqrt{1-e^{-\frac{2\Lambda_3}{(1-\iota_c)\Lambda_1}}},k_{di}\sqrt{1-e^{-2\left(\frac{\Lambda_3}{(1-\iota_c)\Lambda_2}\right)^{\frac{2}{b+1}}}}\right\}\end{aligned}\tag{78}$$

and the total convergence time satisfies following

$$\begin{aligned}T\leq t_0+\max\Bigg\{&\frac{2}{\iota_c\bar{\Lambda}(1-b)}\ln\left(\frac{\iota_c\bar{\Lambda}V^{\frac{1-b}{2}}(t_0)+\Lambda_2}{\Lambda_2}\right),\\ &\frac{2}{\bar{\Lambda}(1-b)}\ln\left(\frac{\bar{\Lambda}V^{\frac{1-b}{2}}(t_0)+\iota_c\Lambda_2}{\iota_c\Lambda_2}\right)\Bigg\}\end{aligned}\tag{79}$$

where t_0 is the initial time. From (78) and (79), it is clear that all the states are bounded and the errors arrive at arbitrarily small bounded regions after a finite time.

ii) Because the compensation signal υ_i is bounded, there is a constant $k_s>0$ such that $|s_i|\leq k_s$. Based on Assumption 1 and $x_1=z_1+y_d=s_1+\upsilon_1+y_d$, we can further know that when k_{d1} is denoted as $k_{d1}=k_{a1}-k_s-Y_1$, then x_1 holds the inequality $|x_1|\leq|s_1|+|\upsilon_1|+|y_d|\leq k_s+k_{d1}+Y_1=k_{a1}$. From Lemma 5, the differentiator's output ϖ_i exists a upper bound $\bar{\varpi}_i$, that is, $|\varpi_i|\leq\bar{\varpi}_i$. Then, it satisfies $|x_2|\leq|s_2|+|\upsilon_2|+|\varpi_2|\leq k_s+k_{d2}+\bar{\varpi}_2=k_{a2}$, if we denote k_{d2} as $k_{d2}=k_{a2}-k_s-\bar{\varpi}_2$. By repeating the previous processes, it follows that the system states are bounded by $|x_j|\leq k_{aj}$, $(j=3,\ldots,n)$, if k_{dj} is denoted as $k_{dj}=k_{aj}-k_s-\bar{\varpi}_j$. According to above discussions and analysis, we can make the conclusion that the constraints of all the system states are never violated, that is, $|x_i|\leq k_{ai}$. As a result, this finishes the proof ii).

Remark 4: In the traditional BC, the multiple differentiations of virtual signals may be impossible to completely avoid, which will cause the "*explosion of complexity*" problem. As we know, although the DSC can handle this problem by applying the FTCF, the filtering-errors caused by the filtering process are inevitable. By additionally introducing the filtering-error compensation system, the aforesaid problems can be overcome and control performance can be improved.

Remark 5: For the ACS designed in this study, the following benefits should be highlighted: (i) Compared with the works [35], [36], the singular issue is completely addressed when ζ is close to the origin; (ii) Different from the works in [32], [36], the saturation-approximation error is rapidly compensated and the output of the ACS is smooth; (iii) Unlike the result [37], the boundedness of Δu is not required.

Remark 6: Compared with the well-known conclusions, the key advantages of our work are summarized by

(1) For the DSC schemes in [3], [14], [20], where the filtering error would reduce the control performance, the filtering error is solved without destroying the finite-time property.
(2) Unlike [24], [25], [30], [40], this study simultaneously considers external perturbations, uncertain functions, full-state constraints, and actuator fault, which makes the proposed framework more reliable for practical engineering.
(3) For the direct NN-based approximation ways in [10], [30], [39], where each component of the optimal NN weight

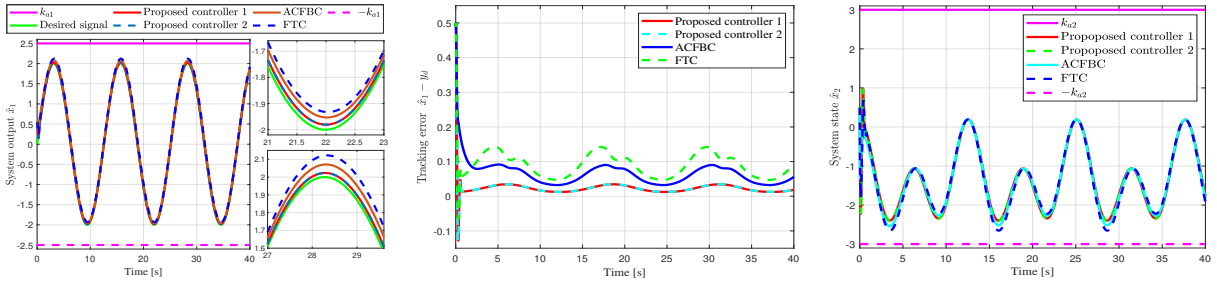

(a) System output under different controllers (b) Tracking error under different controllers (c) System state under different controllers

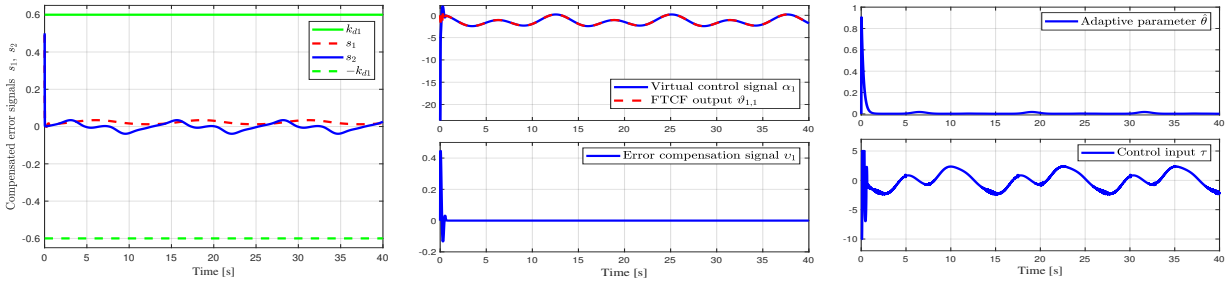

(d) Compensated error signals under proposed controller 1 (e) Virtual signal, FTCF output and error compensation signal under proposed controller 1 (f) Adaptive parameter and control input under proposed controller 1

Fig. 2. Time response of all the signals for *Example 1*.

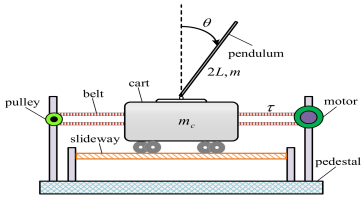

Fig. 3. Physical structure of the inverted pendulum system

needs to be updated online, they will severely consume the limited calculation resource since a large number of NN learning parameters are required to obtain satisfactory approximation results. For this point, this study utilizes the RBFNN technology to approximate $\|F_i\|, (i = 1, \ldots, N)$ rather than F_i, which reduces the number of learning parameters. As a result, the proposed NN method can significantly mitigate the computation burden.

Remark 7: To achieve better control performance, the key guidelines for the parameter choice are summarized as

1) First, the control parameters c_i, h_i, q_i, β_i, and η_i play important roles in dominating the system robustness and the control accuracy. Larger values of those parameters can realize the better control performance.
2) Besides, the adaptation gain γ critically determines the update speed of $\hat{\theta}$. Larger value of γ helps to improve the update speed, however overlarge value may cause the overestimation problem and more energy consumption.
3) What is more, the appropriate choice of the parameter ρ avoids the phenomenon of the parameter drifting, and the parameter b should satisfy $b \in (0, 1)$ and a smaller value of b will contribute to a faster convergence rate.

IV. Result Analysis

To illustrate the effectiveness of the obtained results, four comparative examples are provided in this section.

A. Example 1 (General Second-order System)

Consider a second-order nonlinear system described by

$$\begin{cases} \dot{x}_1 = (0.6x_2 + x_1^2) + (1 + 0.02\sin(x_1))x_2 \\ \qquad +(0.5\cos(t) + 0.2) \\ \dot{x}_2 = (0.2x_1x_2^2 + 0.1) + (1.2 + 0.01\cos(x_2))\tau \\ \qquad +(0.8\sin(t) - 0.1) \end{cases} \tag{80}$$

where $f_1 = 0.6x_2 + x_1^2$, $f_2 = 0.2x_1x_2^2 + 0.1$, $g_1 = 1 + 0.02\sin(x_1)$, $g_2 = 1.2 + 0.01\cos(x_2)$, $d_1 = 0.5\cos(t) + 0.2$, $d_2 = 0.8\sin(t) - 0.1$, and the saturation coefficients are $\bar{u}_r = 5$ and $\underline{u}_r = -10$. The desired signal is set as $y_d = \sin(0.5t) + \cos(t)$, and all states are constrained within $|\hat{x}_1| \leq k_{a1} = 2.5$ and $|\hat{x}_2| \leq k_{a2} = 3$. The different controllers are described by

1) Proposed controller 1: This controller considers the problems of the actuator saturation, external disturbances, and state constraints, and its design parameters are set as $q_1 = 10$, $q_2 = 10$, $p_1 = 1$, $p_2 = 1$, $k_{d1} = 0.6$, $k_{d2} = 0.7$, $b = \frac{19}{21}$, $h_1 = 10$, $h_2 = 10$, $\beta_1 = 30$, $\beta_2 = 30$, $\gamma = 2$, $\rho = 1$, $c_1 = 1$, $c_2 = 1$, $L_1 = 10$, $L_2 = 10$, $\varphi_1 = 0.6$, $\varphi_2 = 1.1$, $s = 30$, $\varsigma_i = 0$, $\nu_i = 2$, and $\hat{x}(0) = \vartheta_{1,1}(0) = \vartheta_{1,2}(0) = \hat{\theta}(0) = \zeta(0) = \upsilon_1(0) = \upsilon_2(0) = 0$.
2) Proposed controller 2: Compared with the proposed controller 1, this controller ignores the actuator saturation problem, and its design values are the same as those of the proposed controller 1. This is to verify that the proposed controller 1 can solve the actuator saturation effectively.
3) Adaptive command filtering backstepping controller [41] (called as ACFBC hereafter) is used as a comparison, to

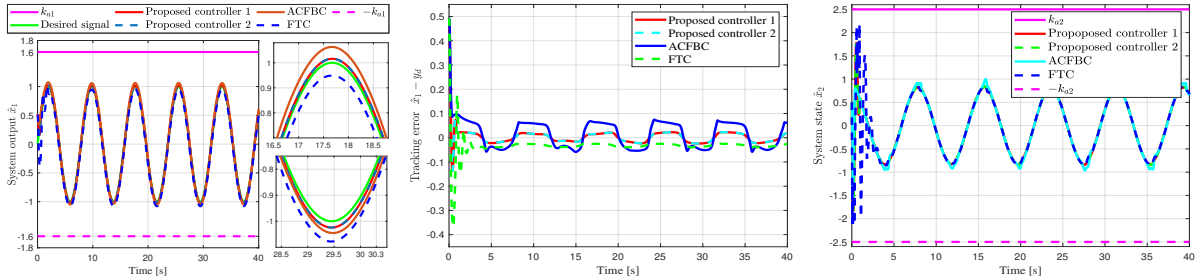

(a) System output under different controllers (b) Tracking error under different controllers (c) System state under different controllers

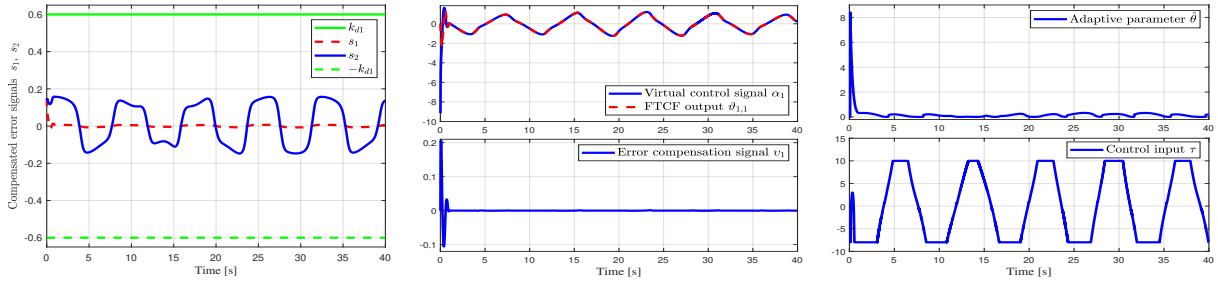

(d) Compensated error signals under proposed controller 1 (e) Virtual signal, FTCF output and error compensation signal under proposed controller 1 (f) Adaptive parameter and control input under proposed controller 1

Fig. 4. Time response of all the signals for *Example 2*.

illustrate the stronger robustness of proposed controller 1, which can be mathematically written as 3.1) Virtual input: $\alpha_1 = \frac{1}{g_1}\big(-\frac{1}{2p_1^2}\frac{s_1^3}{k_{d1}^4 - s_1^4}\hat{\theta}\Xi_1^2 - \frac{3}{4}s_1\big(k_{d1}^4 - s_1^4\big)^{-\frac{1}{3}} - q_1 z_1 - \dot{y}_d\big)$; 3.2) Error-compensation system: $\dot{\upsilon}_1 = -c_1\upsilon_1 + g_1\upsilon_2 + g_1(\varpi_1 - \alpha_1)$ and $\dot{\upsilon}_2 = -c_2\upsilon_2$; 3.3) Actual input: $u = \frac{1}{g_2}\big(-q_2 z_2 - \frac{1}{2p_1^2}\frac{s_2^3}{k_{d2}^4 - s_2^4}\hat{\theta}\Xi_2^2 - \frac{3}{4}s_2\big(k_{d2}^4 - s_2^4\big)^{-\frac{1}{3}}\big)$; 3.4) Adaptive law: $\dot{\hat{\theta}} = \sum_{i=1}^{2}\frac{\gamma}{2p_i^2}\frac{s_i^6}{\big(k_{di}^4 - s_i^4\big)^2}\Xi_i^2 - 2\gamma\rho\hat{\theta}$.

4) Finite-time controller [24] (called as FTC hereafter) is used to infer the fast convergence of proposed controller 1, which is described as: 4.1) Virtual input: $\alpha_1 = \frac{1}{g_1}\big(-\beta_1\big(\frac{z_1}{k_{d1}^2 - z_1^2}\big)^{\frac{b-1}{2}} z_1^{\frac{b+1}{2}} - W_1^{\mathrm{T}}\Xi_1 + \dot{y}_d - \frac{(h_a+3)z_1}{2(k_{d1}^2 - z_1^2)}\big)$; 4.2) Actual input: $u = \frac{1}{g_2}\big(-\beta_2\big(\frac{z_2}{k_{d2}^2 - z_2^2}\big)^{\frac{b-1}{2}} z_2^{\frac{b+1}{2}} - l_2\tilde{x}_2 - W_2^{\mathrm{T}}\Xi_2 - \frac{(k_{d2}^2 - z_2^2)z_1}{k_{d1}^2 - z_1^2} - \frac{z_2}{2(k_{d2}^2 - z_2^2)} + \dot{\alpha}_2\big)$; 4.3) Adaptive laws: $\dot{W}_1 = \frac{\gamma\Xi_1 z_1}{k_{d1}^2 - z_1^2} - \gamma\rho W_1$ and $\dot{W}_2 = \frac{\gamma\Xi_2 z_2}{k_{d2}^2 - z_2^2} - \gamma\rho W_2$.

The comparative results of *Example 1* are plotted in Fig. 2. Among them, Figs. 2 (a) and 2 (b) show that the tracking errors of the proposed controllers are smaller than those of the ACFBC and FTC schemes, and their system outputs satisfy the requirement of the state constraint. From Figs. 2 (c) and (d), it can be observed that the state $\hat{x}_2$ and the compounded error signals s_1 and s_2 are constrained to the required ranges. Fig. 2 (e) displays the curves of the virtual control signal α_1, FTCF's output $\vartheta_{1,1}$, and filtering-error compensation signal υ_1. From Fig. 2 (e), we can know that the designed filtering-error compensation system can effectively compensate for the effect of the filtering error. Fig. 2 (f) shows that the adaptive parameter $\hat{\theta}$ quickly converges to around zero and the control input τ is constrained to the specified range by means of the ACS and an improved Gaussian function. By comparison, it is fully verified that the proposed controller 1 has a better control performance and satisfies the system constraints.

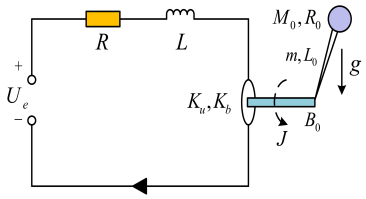

Fig. 5. Physical structure of the single-link manipulator

B. Example 2 (Second-Order Practical System)

We first take into account the inverted pendulum system [31], as shown in Fig. 3, and its dynamics is modeled by

$$\begin{cases} \dot{x}_1 = x_2 \\ \dot{x}_2 = \dfrac{g\sin\theta - \frac{mLx_2^2\cos\theta\sin x_1}{m_c+m}}{L\left(\frac{4}{3} - \frac{m\cos^2 x_1}{m_c+m}\right)} + \dfrac{\frac{\cos x_1}{m_c+m}}{L\left(\frac{4}{3} - \frac{m\cos^2 x_1}{m_c+m}\right)}\tau + d(t) \end{cases} \tag{81}$$

where x_1 and x_2 are the position and velocity of the pendulum angle, respectively; $d(t) = 0.6\cos(t) + \sin(0.5t)$ and τ are the external disturbance, such as rugged slideway and wind-gust disturbance, and the pull force of the motor, respectively; $m_c = 1$ [kg] is the cart's mass, $m = 0.1$ [kg] is the pendulum's mass and $g = 9.81$ [m/s^2]; $L = 1$ [m] is a half of the length of the pendulum. The saturation coefficients are $\bar{u}_r = 8$ and $\underline{u}_r = -10$. The desired signal is $y_d = 2\sin(t) + \cos(0.5t)$ and all states are constrained to $|x_1| \le k_{a1} = 1.6$ and $|x_2| \le k_{a2} = 2.5$. The design parameters are set as $q_1 = 2$, $q_2 = 2$, $p_1 = 10$, $p_2 = 10$, $k_{d1} = 0.8$, $k_{d2} = 0.8$, $b = \frac{13}{15}$, $h_1 = 8$, $h_2 = 8$, $\beta_1 = 5$, $\beta_2 = 5$, $\gamma = 0.1$, $\rho = 1$, $c_1 = 1$, $c_2 = 1$,

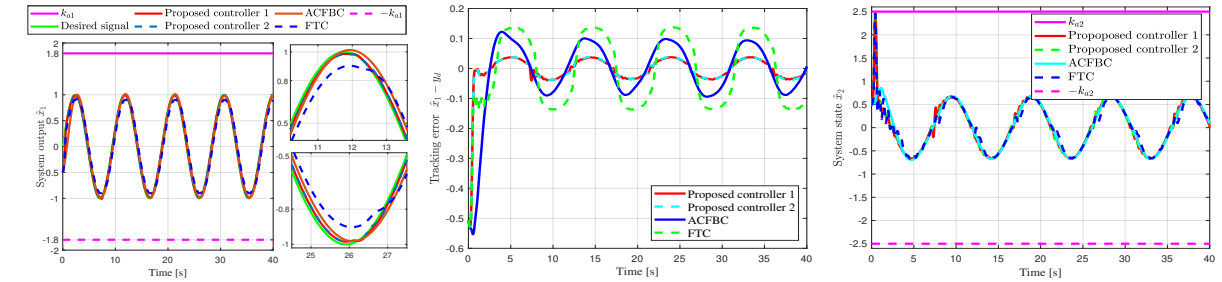

(a) System output under different controllers (b) Tracking error under different controllers (c) System states under different controllers

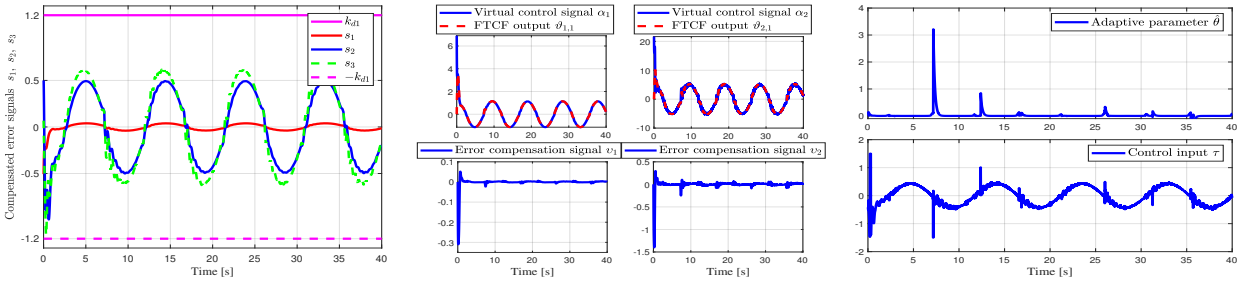

(d) Compensated error signals under proposed controller 1 (e) Virtual signals, FTCF outputs, and error compensation signals under proposed controller 1 (f) Adaptive parameter and control input under proposed controller 1

Fig. 6. Time response of all the signals for *Example 3*.

$L_1 = 10$, $L_2 = 10$, $\varsigma_i = 0$, $\nu_i = 2$, $\vartheta_{1,1}(0) = 0$, $\vartheta_{1,2}(0) = 0$, $\hat{\theta}(0) = 0$, $\zeta(0) = 0$, $\upsilon_1(0) = 0$, and $\upsilon_2(0) = 0$.

Figs. 4 (a) and (b) exhibit the curves of the system output $\hat{x}_1$ and the tracking error $\hat{x}_1 - y_d$, respectively. From Figs. 4 (a) and 4 (b), we can see that the system output of the proposed controller 1 fast tracks y_d and is not violated. Although the system state never exceeds the constraint under the ACFBC and FTC, their convergence rates are solwer than other controllers. As can be found in Fig. 4 (c), the system state $\hat{x}_2$ satisfies its constraint requirement. The trajectories of the compensated error signals s_1 and s_2 are presented in Fig. 4 (d). This reflects the variables s_1 and s_2 satisfy the constraints. The curves of the virtual control signal α_1, FTCF's output $\varrho_{1,1}$, and the error compensation signal υ_1 are given in Fig. 4 (e), which shows that the FTCF can quickly approximate the virtual control signal with high precision. Furthermore, the trajectories of the parameter $\hat{\theta}$ and actual input u are plotted in Fig. 4 (f), which reflects that the boundedness of $\hat{\theta}$ can be ensured and the control input τ holds the saturation constraint.

C. Example 3 (Third-Order Practical System)

As shown in Fig. 5, we consider a single-link manipulator [29], which can be written as

$$\begin{cases} \dot{x}_1 = & x_2 \\ \dot{x}_2 = & \frac{1}{\frac{J}{K_u}+\frac{mL_0^2}{3K_u}+\frac{M_0L_0^2}{K_u}+\frac{2M_0L_0^2}{5K_u}}\left(x_3 - \frac{B_0}{K_u}x_2\right) \\ & -\frac{\frac{mL_0g}{2K_u}+\frac{M_0L_0g}{K_u}}{\frac{J}{K_u}+\frac{mL_0^2}{3K_u}+\frac{mL_0^2}{K_u}+\frac{2mL_0^2}{5K_u}}\sin(x_1) - \frac{R_0x_2x_3^2}{M_0} \\ \dot{x}_3 = & \frac{1}{L}\tau - \frac{K_b}{L}x_2 - \frac{R}{L}x_3 - \frac{R_0x_2\sin x_3}{L} \end{cases} \tag{82}$$

where $[x_1, x_2, x_3]^{\mathrm{T}} = [q, \dot{q}, I]^{\mathrm{T}}$ and $\tau = U_e$ with q, I and U_e being the angular motor position, the armature current, and input voltage; and the physical parameters are set as Back-emf coefficient $K_b = 0.09$ [Nm/A], load radius $R_0 = 0.23$ [m], conversion value $K_u = 0.9$ [Nm/A], viscous friction coefficient $B_0 = 0.01625$ [Nms/rad], rotor inertia $J = 0.1625$ [Kg $\cdot$ m^2], load mass $M_0 = 0.434$ [Kg], link length $L_0 = 0.03$ [m], link mass $m = 0.506$ [Kg], gravity coefficient $g = 9.81$ [N/kg], armature resistance $R = 0.0005$ [Ω], and armature inductance $L = 0.5$ [L]. The saturation coefficients are $\bar{u}_r = 10$ and $\underline{u}_r = -8$. The desired trajectory is $y_d = 0.5(\sin(t) + \sin(0.5t))$ and the boundaries of constrained states are set as $|x_1| \leq k_{a1} = 1.8$, $|x_2| \leq k_{a2} = 2.5$, and $|x_3| \leq k_{a3} = 2.5$. The control parameters are $q_1 = q_2 = q_3 = 0.1$, $p_1 = 10$, $p_2 = 10$, $p_3 = 5$, $k_{d1} = 1.2$, $k_{d2} = 1.2$, $k_{d3} = 1.2$, $b = \frac{199}{201}$, $h_1 = 5$, $h_2 = 5$, $h_3 = 5$, $\beta_1 = 10$, $\beta_2 = 8$, $\beta_3 = 5$, $\gamma = 3$, $\rho = 1$, $\eta_1 = 3$, $\eta_2 = 5$, $c_1 = 2$, $c_2 = 2$, $c_3 = 2$, $L_1 = 10$, $L_2 = 10$, $\varsigma_i = 0$, $\nu_i = 0.5$, and $\vartheta_{1,1}(0) = \vartheta_{1,2}(0) = \vartheta_{2,1}(0) = \vartheta_{2,2}(0) = \hat{\theta}(0) = \zeta(0) = \upsilon_1(0) = \upsilon_2(0) = \upsilon_3(0) = 0$.

Figs. 6 (a) and (b) reflect that the proposed controllers 1 and 2 can fast track the desired signal, their errors are smaller than the ACFBC and FTC, and satisfy the full-state constraints. Despite the presence of actuator saturation, the performance of proposed controller 1 is almost the same as that of the proposed controller 2. This is because when the system encounters the input saturation, the ACS and the improved Gaussian function can solve the input saturation. Figs. 6 (c) and 6 (d) show that under the proposed controller 1, the curves of the compensated error signals s_1, s_2 and s_3 and the system states x_2 and x_3 are not violated for all time. The curves of the virtual control signals α_1 and α_2, FTCF's outputs $\varrho_{1,1}$ and $\varrho_{2,1}$, and error compensation signals υ_1 and υ_2 are plotted in Fig. 6 (e). In addition, Fig. 6 (f) shows the responses of the parameter $\hat{\theta}$ and the control input τ.

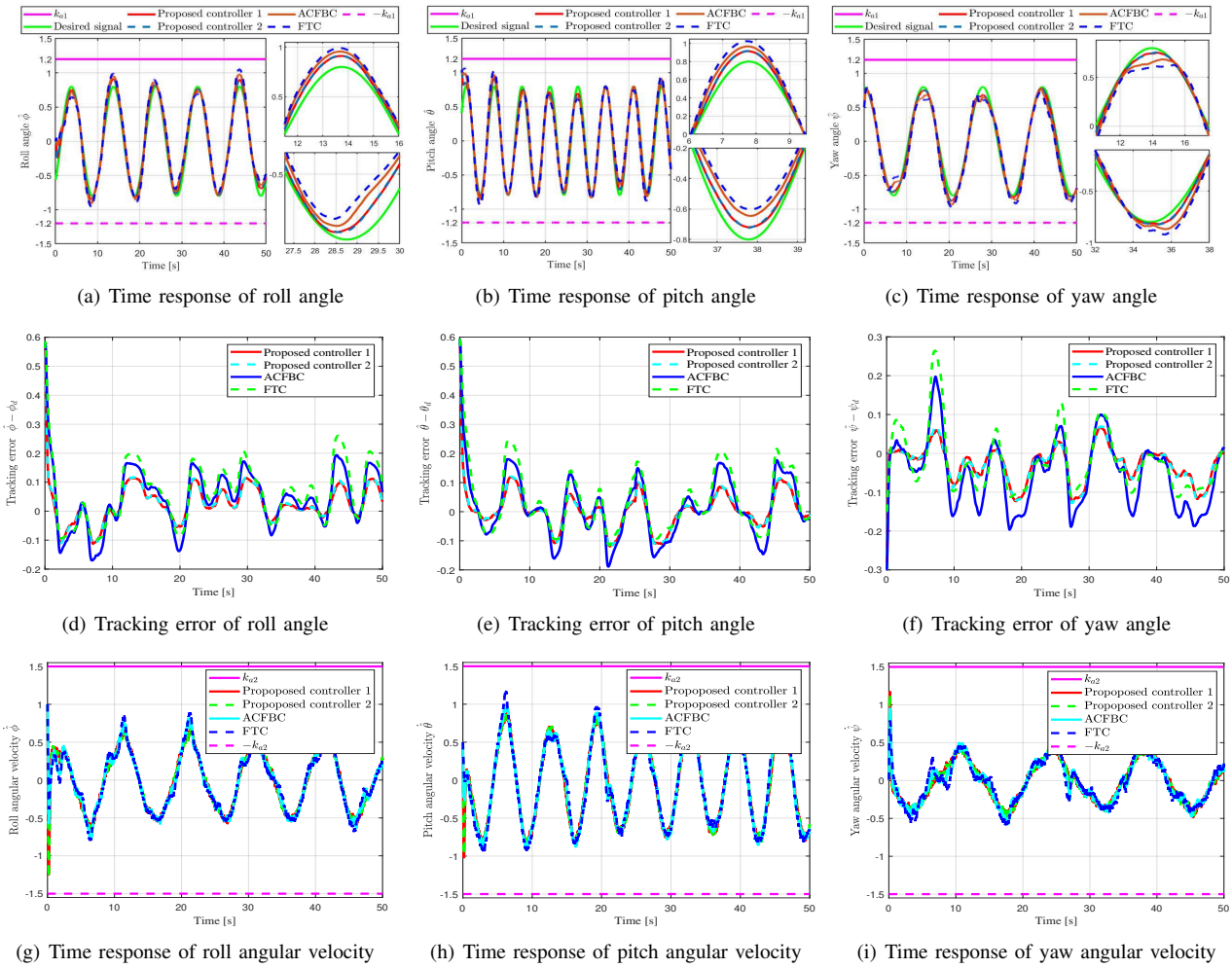

(a) Time response of roll angle (b) Time response of pitch angle (c) Time response of yaw angle

(d) Tracking error of roll angle (e) Tracking error of pitch angle (f) Tracking error of yaw angle

(g) Time response of roll angular velocity (h) Time response of pitch angular velocity (i) Time response of yaw angular velocity

Fig. 7. Time response of all the signals for *Example 4* under different controllers.

D. Example 4 (Quadrotor attitude tracking system)

The attitude dynamics of the quadrotor is formulated as [33]

$$\begin{cases} \ddot{\phi} = \frac{1}{I_\phi}\tau_\phi + \dot{\theta}\dot{\psi}\frac{I_\theta - I_\psi}{I_\phi} - \frac{H_\phi}{I_\phi}\dot{\phi} + \frac{d_\phi}{I_\phi} \\ \ddot{\theta} = \frac{1}{I_\theta}\tau_\theta + \dot{\psi}\dot{\phi}\frac{I_\psi - I_\phi}{I_\theta} - \frac{H_\theta}{I_\theta}\dot{\theta} + \frac{d_\theta}{I_\theta} \\ \ddot{\psi} = \frac{1}{I_\psi}\tau_\psi + \dot{\phi}\dot{\theta}\frac{I_\phi - I_\theta}{I_\psi} - \frac{H_\psi}{I_\psi}\dot{\psi} + \frac{d_\psi}{I_\psi} \end{cases} \tag{83}$$

where ϕ, θ, and ψ stands for the roll, pitch, and yaw angles; I_ϕ, I_θ, and I_ψ represent the inertia parameters; τ_ϕ, τ_θ, and τ_ψ describe the control inputs subject to the actuator saturation; d_ϕ, d_θ, and d_ψ are the unknown disturbances; and H_ϕ, H_θ, and H_ψ denote the aerodynamic drag parameters. Denote $x_{\phi,1} = \phi$, $x_{\theta,1} = \theta$, $x_{\psi,1} = \psi$, $x_{\phi,2} = \dot{\phi}$, $x_{\theta,2} = \dot{\theta}$, and $x_{\psi,2} = \dot{\psi}$, (83) is transformed into the generic model, as

$$\begin{cases} \dot{x}_{i,1} = g_{i,1}x_{i,2} \\ \dot{x}_{i,2} = g_{i,2}\tau_i + f_{i,2} + d_{i,2}, \quad i = \phi, \theta, \psi \end{cases} \tag{84}$$

where $g_{i,1} = 1$, $g_{i,2} = \frac{1}{I_i}$, $d_{i,2} = \frac{d_i}{I_i}$, $f_{\phi,2} = \dot{\theta}\dot{\psi}\frac{I_\theta - I_\psi}{I_\phi} - \frac{H_\phi}{I_\phi}\dot{\phi}$, $f_{\theta,2} = \dot{\psi}\dot{\phi}\frac{I_\psi - I_\phi}{I_\theta} - \frac{H_\theta}{I_\theta}\dot{\theta}$, and $f_{\psi,2} = \dot{\phi}\dot{\theta}\frac{I_\phi - I_\theta}{I_\psi} - \frac{H_\psi}{I_\psi}\dot{\psi}$. The physical parameters are $I_\phi = I_\theta = 0.023$ [kg $\cdot$ m^2], $I_\psi = 0.042$ [kg $\cdot$ m^2], and $H_\phi = H_\theta = H_\psi = 2.4 \times 10^{-7}$ [Ns^2/rad^2]. The desired attitude signals are set as $\phi_d(t) = 0.8\sin(\frac{\pi}{5}t - \frac{\pi}{4})$ [rad], $\theta_d(t) = 0.8\sin(0.3\pi t + \frac{\pi}{6})$ [rad], and $\psi_d(t) = 0.8\cos(0.45t)$ [rad], as well as $\phi(0) = 0$ [rad],$\theta(0) = 1$ [rad], $\psi(0) = 0.5$ [rad], $\dot{\phi}(0) = 1$, $\dot{\theta}(0) = 0.5$ and $\dot{\psi}(0) = 0$ [rad]. The states are constrained as $|\phi| \leq 1.2$, $|\theta| \leq 1.2$, $|\psi| \leq 1.2$, $|\dot{\phi}| \leq 1.5$, $|\dot{\theta}| \leq 1.5$, and $|\dot{\psi}| \leq 1.5$. The control parameters are chosen as $q_{i,1} = q_{i,2} = 3$, $p_{i,1} = p_{i,2} = 6$, $k_{i,d1} = k_{i,d2} = 1.5$, $b = \frac{13}{15}$, $h_{i,1} = h_{i,2} = 5$, $\beta_{i,1} = \beta_{i,2} = 7$, $\gamma_{i,1} = 1$, $\rho_{i,2} = 0.1$, $\eta_{i,1} = \eta_{i,2} = 4$, $c_{i,1} = c_{i,2} = 2$, $L_{i,1} = L_{i,2} = 10$, $\varsigma_i = 0$, $\nu_i = 1$, $\vartheta_{i,1,1}(0) = \vartheta_{i,1,2}(0) = 0$, $\vartheta_{i,2,1}(0) = \vartheta_{i,2,2}(0) = 0$, $\hat{\theta}_i(0) = 0$, $\zeta_i(0) = 0$, and $\upsilon_{i,1}(0) = \upsilon_{i,2}(0) = 0$.

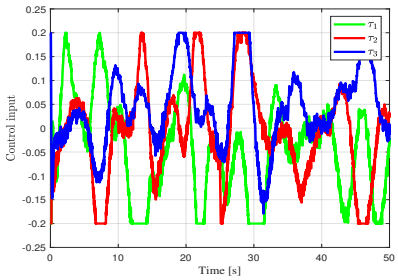

Fig. 8. Time response of control inputs under proposed controller 1

Figs. 7(a)-7(f) show the attitude trajectories and the corre-

TABLE II
PERFORMANCE COMPARISON OF DIFFERENT CONTROLLERS

Mode	Index	Controller			
		Proposed controller 1	Proposed controller 2	ACFBC	FTC
Example 1	μ_{SE}	4.52	4.51	21.88	27.03
	μ_{AE}	95.51	95.28	260.01	359.88
	μ_{TWAE}	1.72×10^5	1.72×10^5	2.71×10^5	6.83×10^5
Example 2	μ_{SE}	4.30	4.25	14.24	40.74
	μ_{AE}	74.51	74.01	204.93	300.68
	μ_{TWAE}	1.30×10^5	1.29×10^5	3.80×10^5	5.18×10^5
Example 3	μ_{SE}	13.93	13.74	54.89	61.15
	μ_{AE}	125.26	124.58	326.61	447.52
	μ_{TWAE}	2.09×10^5	2.08×10^5	5.07×10^5	8.71×10^5
Example 4	μ_{SE}	64.03	62.89	167.87	273.47
	μ_{AE}	684.49	672.64	1240.04	1687.16
	μ_{TWAE}	1.67×10^6	1.64×10^6	3.03×10^6	4.07×10^6

sponding errors of the different controllers, and the proposed controllers 1 and 2 have a better performance than other controllers. Considering the results in Figs. 7 (a)-7 (c), the response of the proposed controller 2 is faster than that of the proposed controller 1 when there is the input saturation. From Figs. 7 (a)-(c) and (g)-(i), it can be found that the constraints of the attitude angles and angular velocities are not violated. Fig. 8 reveals that the proposed controller 1 can handle the input saturation, and control inputs do not exceed their bounds.

Remark 8: Recently, various robust controllers have been successfully used to achieve high-performance control of unmanned aerial vehicles [44]–[46], and their effectiveness has been verified by real experiments. These methods will inspire us in the future to improve the flight effect in different methods. Specifically, a disturbance observer-based sliding mode controller was proposed in [44]. In [45], a robust control-based backstepping technique for the position subsystem and a geometric control for the attitude subsystem were presented to improve system robustness. In [46], the *authors* developed a feedback PID strategy to control the designed fully actuated system. Compared with these methods in [44]–[46], although the proposed method not only ensures that the tracking errors converge to the regions after a finite time but also eliminates the effect of actuator saturation, it is quite difficult to select relatively optimal design parameters in complex experiments, which requires a lot of time and effort.

E. Numerical comparative analysis

In addition to the above curves, specific error data are collected to quantitatively assess the control performance. This study uses three evaluation indices as: (1) Squared error (SE): $\mu_{SE} = \sum_{i=1}^{N}\left(\hat{x}_1(i) - y_d(i)\right)^2$; (2) Absolute error (AE): $\mu_{AE} = \sum_{i=1}^{N}|\hat{x}_1(i) - y_d(i)|$; (3) Time-weighted absolute error (TWAE): $\mu_{TAE} = \sum_{i=1}^{N} i|\hat{x}_1(i) - y_d(i)|$. For the *Example 4*, the evaluation indices are modified as $\mu_{SE} = \sum_{j=1}^{3}\sum_{i=1}^{N}\left(\hat{x}_{j,1}(i) - \phi_d(i)\right)^2$, $\mu_{AE} = \sum_{j=1}^{3}\sum_{i=1}^{N}|\hat{x}_{j,1}(i) - \theta_d(i)|$, and $\mu_{TAE} = \sum_{j=1}^{3}\sum_{i=1}^{N} i|\hat{x}_{j,1}(i) - \psi_d(i)|$.

The quantified data is summarized in Table. II. We can see that the proposed controllers 1 and 2 show a stronger robustness than the ACFBC and FTC. By comparison, the ACFBC has a higher control precision than the FTC, which is because the error-compensation system is integrated into the ACFBC to solve the filtering error. Both the proposed controllers 1 and 2 can realize relatively precise control, but the effect of the proposed controller 2 is better, as can be deduced from the quantitative comparison listed in Table II. In contrast to the proposed controller 2, the proposed controller 1 overcomes the actuator saturation effectively. As a matter of fact, the actuator saturation will prevent from the increase of the control inputs. This inevitably undergoes more program execution time. Fortunately, the control precision is decreased only a little but not significantly. Through the abovementioned discussion, it can be verified that the proposed controller 1 achieves the strong robustness and saturation rejection.

V. CONCLUSION

This article investigates an observer-based adaptive neural FTC scheme for constrained nonlinear systems. First, an NN observer is constructed to observe the immeasurable states. The combination of an improved Gaussian function and ACS is used to solve the actuator saturation. Then, the FTCF and filtering-error compensation system are designed to approximate the virtual signals and address the approximation errors. By applying the NN and virtual parameter learning algorithm, only one adjustable parameter is required. In each controller design procedure, the BLF is incorporated to ensure full the states are never violated and the tracking errors converge to the equilibrium in a finite time. However, the following drawbacks are worth considering: 1) we will focus on how to extend the presented strategy to solve time-varying state constraints instead of constant-state constraints; 2) although the Remark 7 gives a standard guideline for the selection of control parameters, another valuable topic is the study of optimization problems to determine optimal design parameters; and 3) the research of time-varying delays and actuator faults will be explored to improve the system safety and expand the application value in the spacecraft motion [18], [47], intelligent manufacturing [48]–[50], robotic systems [12], [35], etc.

REFERENCES

[1] X. Liu, *et al.*, "A gain-tuning method for almost disturbance decoupling problems of nonlinear systems with zero dynamics," *Int. J. Robust Nonlinear Control*, vol. 32, no. 7, pp. 4459–4476, Feb. 2022.

[2] D. Swaroop, J. K. Hedrick, P. P. Yip, and J. C. Gerdes, "Dynamic surface control for a class of nonlinear systems," *IEEE Trans. Autom. Control*, vol. 45, no. 10, pp. 1839–1899, Oct. 2000.

[3] Z. Peng, Y. Jiang, and J. Wang, "Event-triggered dynamic surface control of an underactuated autonomous surface vehicle for target enclosing," *IEEE Trans. Ind. Electron.*, vol. 68, no. 4, pp. 3402–3412, Apr. 2021.

[4] K. Liu and R. Wang, "Antisaturation command filtered backstepping control-based disturbance rejection for a quadarotor UAV", *IEEE Trans. Circuits Syst. II, Exp. Briefs*, vol. 68, no. 12, pp. 3577–3581, Dec. 2021.

[5] C. Wang, L. Cui, M. Liang, J. Li, and Y. Wang, "Adaptive neural network control for a class of fractional-order nonstrict-feedback nonlinear systems with full-state constraints and input saturation," *IEEE Trans. Neural Netw. Learn. Syst.*, vol. 33, no. 11, pp. 6677–6689, Nov. 2022.

[6] J. A. Farrell, et al., "Command filtered backstepping," *IEEE Trans. Autom. Control,* vol. 54, no. 6, pp. 1391–1395, Jun. 2009.

[7] W. Dong, J. A. Farrell, M. M Polycsrpou, V. Djapic, and M. Sharma, "Command filtered adaptive backstepping," *IEEE Trans. Control Syst. Technol.*, vol. 20, no. 3, pp. 566–580, May 2012.

[8] R. Hao, H. Wang, S. Liu, M. Yang, and Z. Tian, "Multi-objective command filtered adaptive control for nonlinear hydraulic active suspension systems," *Nonlinear Dyn.*, vol. 105, pp. 1559–1579, 2021.

[9] J. Li, et al., "Command filter-based adaptive fuzzy finite-time output feedback control of nonlinear electrohydraulic servo system," *IEEE Trans. Instrum. Meas.*, vol. 71, pp. 3529410, Nov. 2022.

[10] Y. Lian, etc., "Disturbance observer-based adaptive neural network output feedback control for uncertain nonlinear systems", *IEEE Trans. Neural Netw. Learn. Syst.*, vol. 34, no. 10, pp. 7260-7270, Oct. 2023.

[11] C. Xin, Y. -X. Li. and C. L. Ahn, "Adaptive neural asymptotic tracking of uncertain non-strict feedback systems with full-state constraints via command filtered technique", *IEEE Trans. Neural Netw. Learn. Syst.*, vol. 34, no. 10, pp. 5171–5180, Dec. 2023.

[12] G. Li, J. Yu, and X. Chen, "Adaptive fuzzy neural network command filtered impedance control of constrained robotic manipulators with disturbance observer," *IEEE Trans. Fuzzy Syst.*, vol. 34, no. 8, pp. 5171–5180, Aug. 2023.

[13] Y. Yuan and H. Duan, "Adaptive learning control for a quadrotor unmanned aerial vehicle landing on a moving ship," *IEEE Trans. Ind. Informat.*, vol. 20, no. 1, pp. 534-545, Jan. 2024.

[14] L. Wang, H. Wang, and P. X. Liu, "Finite-time compensation control for state-variable-unmeasurable nonlinear systems with sensor and actuator faults," *IEEE Trans. Instrum. Meas.*, vol. 71, pp. 9506308, May. 2022.

[15] B. Chen, H. Zhang, and C. Lin, "Observer-based adaptive neural network control for nonlinear systems in nonstrict-feedback form", *IEEE Trans. Neural Netw. Learn. Syst.*, vol. 27, no. 1, pp. 89–98, Jan. 2016.

[16] W. Ji and J. Qiu, "Observer-based output feedback control of nonlinear 2-D Systems via fuzzy-affine models," *IEEE Trans. Instrum. Meas.*, vol. 71, pp. 3521610, Sept. 2022.

[17] G. Zong, etc., "Observer-based adaptive neural tracking control for a class of nonlinear systems with prescribed performance and input dead-zone constraints," *Neural Netw.*, vol. 147, pp. 126–135, Mar. 2022.

[18] Y. Wang, K. Liu, and H. Ji, "Adaptive robust fault-tolerant control scheme for spacecraft proximity operations under external disturbances and input saturation," *Nonlinear Dyn.*, vol. 108, pp. 207–222, 2022.

[19] K. Liu, et al., "Antisaturation fixed-time attitude tracking control based low-computation learning for uncertain quadrotor UAVs with external disturbances," *Aerosp. Sci. Technol.*, vol. 142, pp. 108668, Nov. 2023.

[20] S. An, M. Chen, H. Wang, and L. Wu, "Fast finite-time dynamic surface tracking control of a single-joint manipulator system with prescribed performance," *Int. J. Syst. Sci.*, vol. 52, no. 8, pp. 1551–1563, Jun. 2021.

[21] S. P. Bhat and D. S. Bernstein, "Continuous finite-time stabilization of the translational and rotational double integrators," *IEEE Trans. Autom. Control*, vol. 43, no. 5, pp. 678–682, May 1998.

[22] E. Moulay, et al., "Finite-time stability and stabilization of time-delay systems," *Syst. Control Lett.*, vol. 57, no. 7, pp. 561–566, 2008.

[23] B. Guo, S. Dian, and T. Zhao , "Event-driven-observer-based fuzzy fault-tolerant control for nonlinear system with actuator fault," *Nonlinear Dyn.*, vol. 107, pp. 3505–3519, 2022.

[24] H. Zhang, Y. Liu, and Y. Wang, "Observer-based finite-time adaptive fuzzy control for nontriangular nonlinear systems with full-state constraints," *IEEE Trans. Cybern.*, vol. 51, no. 3, pp. 1110–1120, Mar. 2021.

[25] J. Yu, P. Shi, W. Dong, and C. Lin, "Adaptive fuzzy control of nonlinear systems with unknown dead zones based on command filtering," *IEEE Trans. Fuzzy Syst.*, vol. 26, no. 1, pp. 46–55, Feb. 2018.

[26] C. Wen, et al., "Robust adaptive control of uncertain nonlinear systems in the presence of input saturation and external disturbance," *IEEE Trans. Autom. Control,* vol. 56, no. 7, pp. 1672–1678, Jul. 2011.

[27] S. Liu, T. Li, and H. Wang, "Fast finite-time command filter-based adaptive composite tracking control for nonlinear systems," *Nonlinear Dyn.*, vol. 111, pp. 3393–3409, 2023.

[28] K. Liu, et al, "Antisaturation finite-time attitude tracking control based observer for a quadrotor", *IEEE Trans. Circuits Syst. II, Exp. Briefs*, vol. 68, no. 6, pp. 2047–2051, June 2021.

[29] H. Wang, K. Xu, P. X. Liu, and J. Qiao, "Adaptive fuzzy fast finite-time dynamic surface tracking control for nonlinear systems," *IEEE Trans. Circuits Syst. I, Reg. Papers*, vol. 68, no. 10, pp. 4337–4348, Oct. 2021.

[30] J. Sun, H. He, J. Yi, and Z. Pu, "Finite-time command-filtered composite adaptive neural control of uncertain nonlinear systems," *IEEE Trans. Cybern.*, vol. 52, no. 7, pp. 6809–6821, Jul. 2022.

[31] W. Wei and W. Zhang, "Command-filter-based adaptive fuzzy finite-time output feedback control for state-constrained nonlinear systems with input saturation", *IEEE Trans. Fuzzy Syst.*, vol. 30, no. 10, pp. 4044–4056, Oct. 2022.

[32] J. Ma, S. S. Ge, Z. Zheng, and D. Hu, "Adaptive NN control of a class of nonlinear systems with asymmetric saturation actuators," *IEEE Trans. Neural Netw. Learn. Syst.*, vol. 26, no. 7, pp. 1532–1538, Jul. 2015.

[33] K. Liu, P. Yang, R. Wang, L. Jiao, T. Li, and J. Zhang, "Observer-based adaptive fuzzy finite-time attitude control for quadrotor UAVs," *IEEE Trans. Aerosp. Electron. Syst.*, vol. 59, no. 6, pp. 8637-8654, Dec. 2023.

[34] K. Liu and R. Wang, "Antisaturation adaptive fixed-time sliding mode controller design to achieve faster convergence rate and its application", *IEEE Trans. Circuits Syst. II, Exp. Briefs*, vol. 69, no. 8, pp. 3555–3559, Aug. 2022.

[35] J. Li, X. Xiang, and S. Yang, "Robust adaptive neural network control for dynamic positioning of marine vessels with prescribed performance under model uncertainties and input saturation," *Neurocomputing*, vol. 484, pp. 1–12, 2022.

[36] X. Fang, et al., "Adaptive finite-time fault-tolerant control of uncertain systems with input saturation," *IEEE Trans. Syst., Man, Cybern., Syst.*, vol. 53, no. 1, pp. 165–177, Jan. 2023.

[37] M. Chen, et al., "Multiapproximator-based fault-tolerant tracking control for unmanned autonomous helicopter with input saturation," *IEEE Trans. Syst., Man, Cybern., Syst.*, vol. 52, no. 9, pp. 5710–5722, Sept. 2022.

[38] K. P. Tee, S. S. Ge, and E. H. Tay, "Barrier Lyapunov functions for the control of output-constrained nonlinear systems," *Automatica*, vol. 45, no. 4, pp. 918–927, 2009.

[39] Z. Zhao, J. Zhang, Z. Liu, C. Mu, and K. -S. Hong, "Adaptive neural network control of an uncertain 2-DOF helicopter with unknown backlash-like hysteresis and output constraints", *IEEE Trans. Neural Netw. Learn. Syst.*, vol 34, no. 12, pp. 10018-10027, Dec. 2023.

[40] J. Liu, et al., "Almost fast finite-time adaptive tracking control for a class of full-state constrained purefeedback nonlinear systems," *Int. J. Robust Nonlinear Control*, vol. 30, no. 17, pp. 7517–7532, Nov. 2020.

[41] Q. Jiang, J. Liu, J. Yu, and C. Lin, "Full state constraints and command filtering-based adaptive fuzzy control for permanent magnet synchronous motor stochastic systems," *Inf. Sci.*, vol. 567, pp. 298–311, Aug. 2021.

[42] Z. Tang, et al., "Robust adaptive neural tracking control for a class of perturbed uncertain nonlinear systems with state constraints," *IEEE Trans. Syst., Man, Cybern. Syst.*, vol. 46, no. 12, pp. 1618–1629, 2016.

[43] A. Levant, "Higher-order sliding modes, differentiation and outputfeed-back control," *Int. J. Control*, vol. 76, no. 9–10, pp. 924–941, 2003.

[44] T. Xie, B. Xian, X. Gu, J. Hu, and M. Liu, "Disturbance observer-based fixed-time tracking control for a tilt trirotor unmanned aerial vehicle", *IEEE Trans. Ind. Electron.*, vol. 71, no. 4, pp. 3894-3903, Apr. 2024.

[45] G. Flores, A. M. de Oca, and A. Flores, "Robust nonlinear control for the fully actuated hexa-rotor: Theory and experiments", *IEEE Control Syst. Lett.*, vol. 7, pp. 277-282, 2023.

[46] A. Flores and G. Flores, "Fully actuated Hexa-rotor UAV: Design, construction, and control. Simulation and experimental validation", in *Proc. Int. Conf. Unmanned Aircr. Syst.*, June 2022, pp. 1497–1503.

[47] K. Liu, *et al.*, "Adaptive saturated tracking control for spacecraft proximity operations via integral terminal sliding mode technique", *Int. J. Robust Nonlinear Control*, vol. 31, no. 18, pp. 9372–9396, Sept. 2021.

[48] J. Leng, *et al.*, "ManuChain II: Blockchained smart contract system as the digital twin of decentralized autonomous manufacturing toward resilience in industry 5.0," *IEEE Trans. Syst., Man, Cybern. Syst.*, vol. 53, no. 8, pp. 4715–4728, Aug. 2023.

[49] J. Leng, W. Sha, Z. Lin, J. Jing, and Q. Liu, "Blockchained smart contract pyramid-driven multi-agent autonomous process control for resilient individualised manufacturing towards industry 5.0," *Int. J. Prod. Res.*, vol. 61, no. 3, pp. 4302–4321, 2023.

[50] J. Leng, *et al.*, "Cloud-edge orchestration-based bi-level autonomous process control for mass individualization of rapid printed circuit boards prototyping services," *J. Manuf. Syst.*, vol. 63, pp. 143–161, Apr. 2022.